


# Retentiveness of rare earth elements in garnet with implications for garnet Lu-Hf chronology

Matthijs A. Smit<sup>1,2</sup> | Johannes C. Vrijmoed<sup>3</sup> | Erik E. Scherer<sup>4</sup> |  
Klaus Mezger<sup>5</sup> | Ellen Kooijman<sup>2</sup> | Melanie Schmitt-Kielman<sup>2</sup> |  
Lorraine Tual<sup>1,2,6</sup> | Carl Guilmette<sup>7</sup>  | Lothar Ratschbacher<sup>8</sup>

<sup>1</sup>Department of Earth, Ocean and Atmospheric Sciences, University of British Columbia, Vancouver, British Columbia, Canada

<sup>2</sup>Department of Geosciences, Swedish Museum of Natural History, Stockholm, Sweden

<sup>3</sup>Department of Earth Sciences, Freie Universität Berlin, Berlin, Germany

<sup>4</sup>Institut für Mineralogie, Universität Münster, Münster, Germany

<sup>5</sup>Institut für Geologie, Bern, Switzerland

<sup>6</sup>Geo-Ocean, Univ Brest, CNRS, Ifremer, UMR6538, Plouzané, France

<sup>7</sup>Département de Géologie et de Génie Géologique, Université Laval, Québec City, Québec, Canada

<sup>8</sup>Institut für Geologie, Technische Universität Bergakademie Freiberg, Freiberg, Germany

## Correspondence

Matthijs A. Smit, Department of Earth, Ocean and Atmospheric Sciences, University of British Columbia, 2020-2207 Main Mall, Vancouver, British Columbia, Canada, V6T 1Z4.  
Email: [msmit@eoas.ubc.ca](mailto:msmit@eoas.ubc.ca)

## Funding information

Vetenskapsrådet; Natural Sciences and Engineering Research Council of Canada, Grant/Award Numbers: RGPIN-2020-04692, Accelerator Grant RGPAS-2020-00069; Swedish Research Council, Grant/Award Numbers: National Infrastructure Grant 2017-00671, International Postdoc grant 2018-00200; European Union's Horizon 2020,

## Abstract

Incorporation of rare earth elements (REE) in garnet enables garnet chronology (Sm-Nd, Lu-Hf), and imparts a garnet-stable signature on cogenetic phases, which allows petrochronology and general petrogenetic tracing of garnet stability in minerals and melts. Constraints on the uptake and redistribution mechanisms, as well as on the diffusive behaviour of REE in garnet are required for allowing accurate interpretation of REE signatures and ages. Garnet REE profiles are often measured to gain insight into the nature and cause of REE zoning. Interpretation of such profiles is nevertheless complicated by poor constraints on the extent of diffusive relaxation. This is especially relevant for Lu, which, according to experiments, has a relatively high diffusivity and thus may re-equilibrate with possible consequences for Lu-Hf chronology. To provide new insight into the REE systematics of garnet, we applied quantitative trace-element mapping of garnet grains from metamorphic rocks that record peak temperatures above 750°C and cooling rates as low as 1.5°C Ma<sup>-1</sup>. Garnet in all samples preserves Rayleigh-type or oscillatory growth zoning with sharply defined interfacial angles that match the garnet habit. Re-equilibration of REE compositions appears restricted to domains with nebulous and patchy zoning, which likely form by interface-coupled dissolution and re-precipitation reactions mediated by fluids or melts, rather than REE volume diffusion. The possible effect of Lu diffusion in the analysed grains was investigated by comparing the observations to the results from 2D numerical modelling using Lu diffusivities from recent diffusion experiments. This test indicates that Lu diffuses significantly slower in natural garnet than experiments predict. The retentiveness of REE in garnet demonstrates the reliability of REE signatures in magmatic tracing and petrochronology and establishes Lu-Hf chronology as a robust means of dating garnet growth and recrystallization in metamorphic rocks, including those that underwent high- or ultrahigh-temperature conditions.

This is an open access article under the terms of the [Creative Commons Attribution](https://creativecommons.org/licenses/by/4.0/) License, which permits use, distribution and reproduction in any medium, provided the original work is properly cited.

© 2024 The Authors. *Journal of Metamorphic Geology* published by John Wiley & Sons Ltd.

Grant/Award Number: Marie Skłodowska-Curie grant 899546; Deutsche Forschungsgemeinschaft, Grant/Award Number: 235221301/C09

Handling Editor: Dr. Sarah Penniston-Dorland

## KEYWORDS

diffusion, garnet, Lu-Hf, rare earth elements, trace element mapping

## 1 | INTRODUCTION

Garnet is the most important petrogenetic indicator mineral in the Earth's crust and mantle and can trace tectonic and magmatic processes through its ability to record pressure ( $P$ ), temperature ( $T$ ), chemical conditions, and time. Almandine-, pyrope-, and spessartine-type garnet, which are the most common garnet varieties in most geological systems, have relatively high partition coefficients for heavy REE (Tb-Lu; HREE) and some middle REE (Nd-Gd; MREE). As such, the concentrations of these elements in rocks and minerals can indicate whether, when, and under which physico-chemical conditions garnet was stable in a given system. For instance, the REE patterns of magmatic rocks can be used to test for residual garnet in the source and thus high melting pressure, whereas in metamorphic rocks, they can help trace garnet-forming and consuming reactions, enabling the reconstruction of metamorphic histories (e.g., Hickmott et al., 1987; Pyle & Spear, 2000; Konrad-Schmolke et al., 2008; Moore et al., 2013; George et al., 2018; Konrad-Schmolke et al., 2022). Petrogenetic linkage using REE provides the foundation for the indirect dating of garnet growth and recrystallization via micro-analysis of accessory minerals that are suitable for chronometry, for example, monazite and zircon. The partition coefficients for HREE between these phases have been quantitatively constrained (Hermann & Rubatto, 2003; Rubatto & Hermann, 2007; Taylor et al., 2015). Linking ages of accessory minerals to garnet growth using such constraints has become common practice in the tectonic analysis of orogenic belts (e.g., Foster et al., 2004; Holder et al., 2015; Kohn et al., 2005; Larson et al., 2013; Regis et al., 2016; Warren et al., 2019). The compositions and zoning for REE, as well as other elements that are used as chemical tracers for specific mineral reactions (e.g., P, Cr, Ti, and Zr), provide an opportunity to investigate the petrological history of rocks. However, interpreting these compositional records is not trivial. Growth zoning can reflect Rayleigh fractionation during growth, with compositional changes reflecting changes in garnet growth rate, element supply and uptake by cogenetic minerals, and the kinetics of element transport in the intergranular medium (Carlson, 2012; George et al., 2018; Hollister, 1966; Konrad-Schmolke et al., 2008; Otamendi et al., 2002; Skora et al., 2006). The primary

zoning may be locally modified or truncated by interface-coupled dissolution-precipitation, both statically and during deformation (e.g., Ague & Axler, 2016; Smit et al., 2011). Superimposed on all of these features may be the effects of diffusive zoning relaxation. Constraints on REE diffusivity in garnet are required to properly assess the effects of this process on garnet REE compositions and zoning, on rock-wide REE (re-)distribution, and on Sm-Nd and Lu-Hf ages. An extensive effort has been invested in experimentally constraining REE diffusivity in garnet ( $D_{\text{REE}}$ ; e.g., Ganguly et al., 1998; van Orman et al., 2002; Tirone et al., 2005; Bloch et al., 2015, 2020). Estimates of  $D$  for a given REE at a given  $T$  can differ by orders of magnitude between studies. These differences may reflect differences in experimental design—different measurement techniques, oxygen fugacity and garnet composition—but may also indicate different rate-limiting mechanisms at different physical or chemical conditions. Among the extremes is a ‘fast’ diffusion mechanism, which was detected in a recent diffusion experiment run at 1 atm and is associated with diffusivities that are at least two orders of magnitude higher at geologically relevant temperatures than those constrained in most other experiments (Bloch et al., 2020). An experiment run at 1 GPa in the same study indicates significantly more sluggish diffusion at high pressure. The ‘fast’ mechanism was nevertheless suggested to be of significance at any  $P$  less than 1 GPa and thus to apply in many metamorphosed rocks (Bloch et al., 2020). Diffusion modelling of major- and trace-element zoning in garnet xenocrysts in granodiorite (~0.3 GPa) provides no indication for this ‘fast’ mechanism (Devoir et al., 2021). Whether this means that this mechanism unilaterally does not occur in natural garnet, or whether this particular case provides an exception to a rule is not clear. Observations made from natural garnet generally indicate that REE diffusion in natural garnet is relatively sluggish. Garnet that has undergone long-lived thermal overprinting during high and ultrahigh-temperature (HT; UHT) metamorphism commonly preserves strong REE zoning (e.g., Carlson, 2012; Cutts & Smit, 2018; Guilmette et al., 2018; Guilmette et al., 2023; Pownall et al., 2019; Pyle & Spear, 2000; Rubatto et al., 2020; Smit, Ratschbacher, et al., 2014). Estimates of REE diffusivities constrained from diffusion zoning in natural garnet are

lower than those determined in most experiments (Carlson, 2012) and are approximated only by REE diffusivities determined in a high-pressure diffusion experiment (van Orman et al., 2002).

The uncertainty regarding REE diffusivity poses a substantial issue in garnet geochronology, especially for the Lu-Hf system where the parent element (Lu) has a higher diffusivity than the daughter element (Hf). Changes in the Lu budget of garnet as a result of diffusive Lu exchange with the matrix could affect age systematics, potentially causing Lu-Hf isochrons that are associated with elevated mean squared weighted deviation (MSWD) values, and imprecise and spurious ages (Bloch et al., 2020; Bloch & Ganguly, 2015; Kohn, 2009). The degree to which such effects are reflected in global Lu-Hf data is not clear; neither MSWD nor age uncertainties are necessarily higher for higher-temperature metamorphic rocks (Figure 1). With no clear exception, and regardless of rock composition, mineral assemblage or metamorphic grade, Lu-Hf garnet ages are similar to, or older than, the accessory mineral U-Pb ages that are interpreted to date peak metamorphism (Figure 1b). The data thus do not reflect downskewing of Lu-Hf ages, as predicted for garnet-clinopyroxene assemblages (Bloch et al., 2015), and in fact can be readily interpreted to reflect the nature of garnet as a prograde mineral that typically forms earlier in the petrogenetic history of metamorphic rocks than zircon or monazite (e.g., Anczkiewicz et al., 2007; Godet et al., 2021; Guilmette et al., 2018; Guilmette et al., 2023; Smit, Hacker, & Lee, 2014) and may even retain age information on metamorphic events that accessory minerals appear to have missed (e.g., Lihter et al., 2022; Thiessen et al., 2019). Although these data generally indicate the robustness of Lu-Hf ages, they do not exclude that Lu diffusion affects such ages in individual cases. Testing for the effects of Lu zoning in given cases relies on the interpretation of Lu zoning. Such interpretation, however, is often inconclusive, because different processes may lead to the same zoning. Kinetic limitations to REE supply in the matrix during growth may, for instance, produce smooth compositional zoning (e.g., Skora et al., 2006) that could easily be misinterpreted to indicate an arbitrary amount of diffusive relaxation. Interpretations of Lu zoning as growth zoning (e.g., Cutts & Smit, 2018; Johnson et al., 2018; Thiessen et al., 2019) may reasonably be questioned because initial Lu concentrations can never be known (Bloch et al., 2020). By the same argument, however, smooth or absent REE zoning (e.g., Ibañez-Mejía et al., 2018; Johnson et al., 2018), which may be interpreted as ‘essentially homogenized’ (Bloch et al., 2020), may still be primary. Examples where cogenetic garnet grains from the same terrane (Lihter et al., 2022) or even the same outcrop (Cutts et al., 2020) show vastly different REE zoning—very

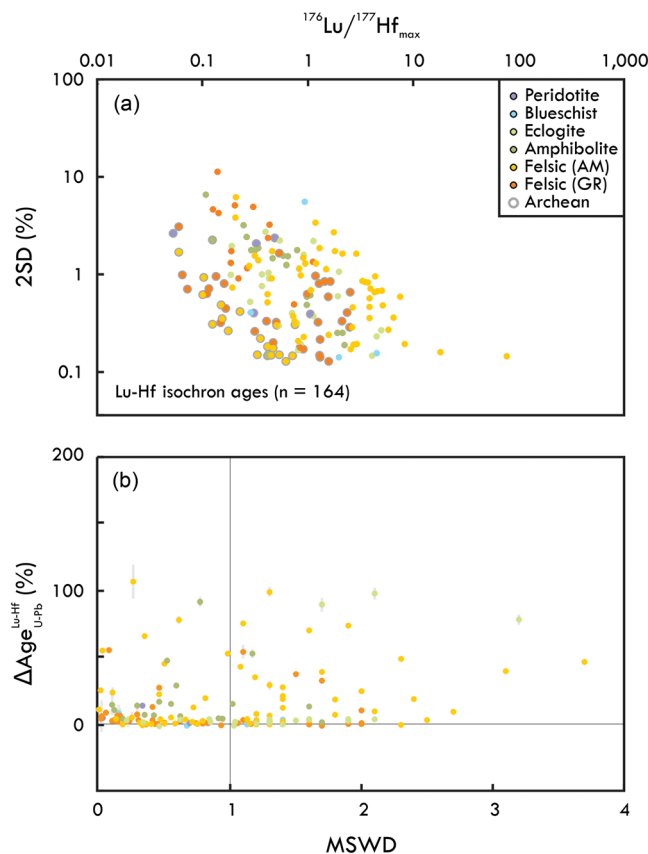


**FIGURE 1** Lu-Hf garnet data collected during the past decade by a single operator in three laboratories using the same analytical protocol. (a) Lu-Hf age uncertainty as a function of maximum garnet  $^{176}\text{Lu}/^{177}\text{Hf}$ . Rocks of higher metamorphic grade do not show systematically higher uncertainty, as would be expected in the case of diffusion-induced age skewing. Instead, age uncertainties broadly correlate with  $^{176}\text{Lu}/^{177}\text{Hf}_{\text{max}}$ , with additional uncertainty likely caused by true geologic scatter. (b) The difference between the Lu-Hf age of garnet and the peak-metamorphic age inferred from accessory mineral U-Pb ( $\Delta\text{Age}_{\text{Lu-Hf}} / \Delta\text{Age}_{\text{U-Pb}}$ ) as a function of MSWD to test whether systematic age differences occur for rocks of different grade or composition. In all cases, samples of different composition and grade show the same characteristic scatter and differences to U-Pb age data, providing no systematic indication for any  $T$ - or composition-controlled age skewing from Lu diffusion.

strong versus smooth and seemingly re-homogenized—capture the essence of this conundrum.

Trace-element mapping of metamorphosed garnet provides an avenue for investigating REE systematics in garnet because it reveals features of REE zoning that, in only one dimension, might remain undetected. Specifically, this technique allows more reliable interpretation of zoning, even in cases where compositional gradients along core-to-rim profiles are relatively smooth. For instance, concentric growth zoning may mimic the garnet habit, preserving sharply defined interfacial angles, whereas diffusive relaxation would round off the corners of such zoning and may further perturb original zoning during resorption.

Mapping of REE in garnet has long posed an analytical challenge because electron-probe micro-analysers are not sensitive enough. This issue is now overcome through innovations in laser ablation inductively coupled plasma mass spectrometry (LA-ICPMS), for example, two-volume ablation cells with sub-second aerosol evacuation, and improved analytical and data-reduction strategies. Trace-element concentrations can now be mapped at the parts-per-million level and micron-scale spatial resolution, providing a new avenue for investigating garnet growth and element uptake (e.g., Gaidies et al., 2021; George et al., 2018; Guilmette et al., 2018; Raimondo et al., 2017; Rubatto et al., 2020). In this study, this analytical approach is used to obtain trace-element maps for garnet grains in various *HT* metamorphic rocks. Specific focus is on the REE, as well as Cr, which is relatively immobile in garnet and hence may serve as benchmark for detecting growth zoning (Carlson, 2012; Martin, 2009). The analysed samples include a slowly cooled Neoproterozoic felsic granulite from the Pikwitonei Granulite Domain, SW Superior Province (Manitoba, Canada), a Caledonian ultrahigh-pressure migmatite from the Western Gneiss Complex, W. Norway, a clinopyroxene-garnet granulite from the metamorphic sole of the Semail Ophiolite in Oman, and a mafic granulite from one of the world's largest core complexes, exposed in the Pamir, Tajikistan. Each of these samples records a thermal history that is on the extreme end of what is known for crustal settings. To investigate the differences between expected and observed REE zoning in these grains, we compared the results from these maps to those from the numerical modelling of element diffusion in two-dimensional space. The results yield new insight into the diffusive behaviour of REE in garnet and the differences in REE diffusivity between nature and experiment. In doing so, the results improve the usefulness of garnet as a tool in the investigation of igneous and metamorphic rocks by (1) allowing more effective use of REE compositions in garnet in solving petrological histories, (2) improving our ability to link garnet and accessory minerals through REE for the purpose of petrochronology, and (3) facilitating a more reliable interpretation of garnet Lu-Hf and Sm-Nd ages.

## 2 | GEOLOGICAL SETTING AND SAMPLE DESCRIPTIONS

### 2.1 | Felsic granulite 407—Pikwitonei Granulite Domain (Manitoba, Canada)

The Pikwitonei Granulite Domain (PGD) represents the highest-grade part of a section across the Archean basement of the NW Superior Province, Manitoba, Canada.

To the north and west, the PGD is enveloped by the Thompson Nickel Belt. This structure is part of a network of lithosphere-scale shear zones of the Trans-Hudson Orogen, which separates the Superior and Hearne Cratons. The Thompson Nickel Belt contains 1.88 to 1.86 Ga mafic and ultramafic intrusions with associated Ni-Cu-PGE mineralization, which were subjected to amphibolite facies metamorphism and deformation at c. 1.76 Ga (Scoates et al., 2017). To the southwest, the PGD borders the Oxford-Stull Domain of the North Caribou Superterrane, which is dominated by 3.0 to 2.9 Ga basement granitoids with infolded greenstone belts, all typically metamorphosed at amphibolite facies conditions (Percival et al., 2006). The PGD is set in the Northern Superior superterrane, which consists of c. 3.5 Ga orthogneiss and granites, and 3.2 to 3.1 Ga tonalite-trondhjemite-granodiorite complexes. The PGD records increasing peak-metamorphic conditions, from  $\sim 760^\circ\text{C}$  and 0.8 GPa at the boundary with the Oxford-Stull Domain to over  $900^\circ\text{C}$  and 0.9 GPa in the highest-grade west and northwest areas, with no visible tectonic breaks (Guevara et al., 2020; Kooijman et al., 2012; Mezger et al., 1990; Weber & Scoates, 1978). Early metamorphism is recorded by c. 2.716 Ga zircon growth in mafic granulites in the western PGD (Heaman et al., 2011) and c. 2.71 Ga garnet growth in the east (Mezger et al., 1989a; Smit et al., 2013a). This episode was the start of a long-lived metamorphic history, involving several episodes of zircon growth, most prominently at c. 2.695, 2.675, and 2.640 Ga (Guevara et al., 2020; Heaman et al., 2011; Mezger et al., 1989a), with the second of these most likely dating peak granulite facies metamorphism. At Cauchon Lake, metamorphism and migmatization occurred at c. 2.640 Ga, as indicated by high-precision U-Pb analysis of inclusions in garnet within leucocratic segregations in a migmatite and zircon in amphibolite-hosted leucosomes (Heaman et al., 2011; Mezger et al., 1989a). Peak metamorphism of rocks just beyond, that is, northwest of, the orthopyroxene-in isograd occurred at  $\sim 760^\circ\text{C}$  and 0.70–0.75 GPa at c. 2.64 Ga (Kooijman et al., 2012; Mezger et al., 1990), indicating that granulites in this domain underwent at least 70 million years of *HT* metamorphism. Following the intrusion of biotite granites and late pegmatites in the wake of this last metamorphic episode (Mezger et al., 1989a), the PGD underwent a long history of cooling. Rutile U-Pb dating by conventional whole-grain analysis and by LA-ICPMS indicates cooling through  $\sim 500^\circ\text{C}$  at 2.35 Ga in the Cauchon Lake area and at c. 2.25 Ga in the higher grade northwestern PGD (Kooijman et al., 2010; Mezger et al., 1989b). These constraints indicate extremely slow, presumably erosion-driven exhumation and cooling at average rates of  $0.5\text{--}2.2^\circ\text{C Ma}^{-1}$ .



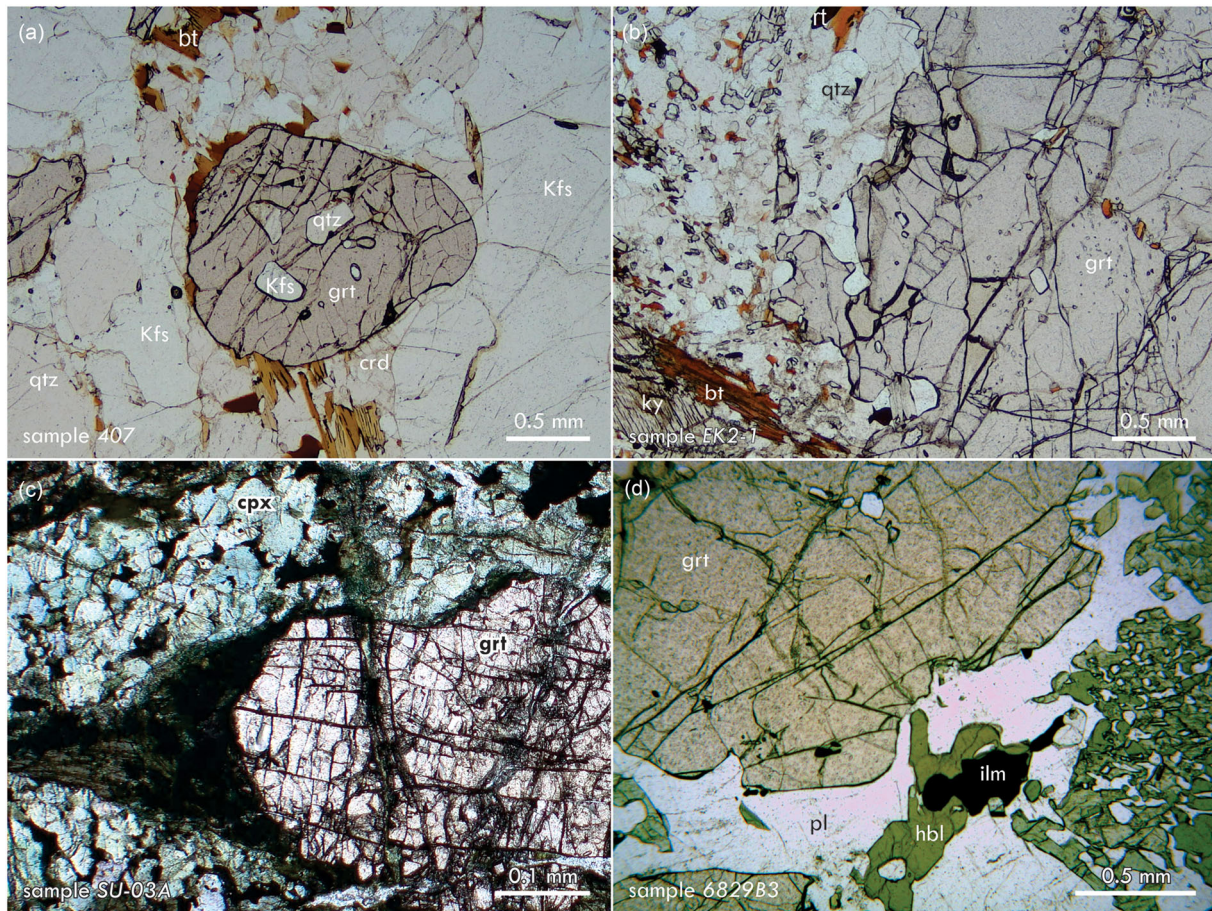


**FIGURE 2** Plane polarized-light images of the samples analysed in this study: (a) Pikwitonei Granulite Domain sample 407, (b) Western Gneiss Complex migmatite *EK2-1*, (c) Semail Ophiolite sole sample *SU-03A*, and (d) Shakhdara dome sample *6829B3*. Abbreviations: bt = biotite, hbl = hornblende, cpx = clinopyroxene, ilm = ilmenite, Kfs = K-feldspar, pl = plagioclase, qtz = quartz.

Sample 407 was collected northwest of the orthopyroxene-in isograd at Cauchon Lake ( $55^{\circ}27'11.66''\text{N}$ ,  $11^{\circ}19'51.85''\text{E}$ ; Smit et al., 2013a). The sample is a felsic migmatite, comprising biotite-, plagioclase-, and quartz-bearing melanosomes interlayered with garnet-, sanidine-, and quartz-dominated leucosomes (Figure 2a). Inclusions in garnet comprise a variety of prograde- to peak-metamorphic minerals, including hercynite, cordierite, and accessory plagioclase, zircon, rutile, and monazite. Garnet formed as a restitic phase from biotite-dehydration melting reactions that consumed cordierite during prograde metamorphism at  $\sim 650^{\circ}\text{C}$  and subsequently underwent peak temperatures of  $\sim 760^{\circ}\text{C}$  (Kooijman et al., 2012; Smit et al., 2013b). Garnet exhibits a large grain-size range (radii  $\sim 0.2\text{--}5\text{ mm}$ ). This study focuses on one of the larger grains from this sample ( $r = 2\text{ mm}$ , grain X of Smit et al., 2013b). The grain exhibits a relatively homogeneous major-element composition of  $\text{alm}_{49-63}\text{prp}_{35-47}\text{grs}_{3-6}\text{sps}_1$  (alm = almandine; prp = pyrope; grs = grossular; sps = spessartine; numbers indicate end-member mol%). The MgO concentration increases gradually from core to

rim, whereas FeO is homogeneous; CaO concentrations decrease, first steadily and then with a steeper gradient towards the rim—features that are attributed to widespread diffusive relaxation (Smit et al., 2013b). Trace-element spot analysis by LA-ICPMS showed bell-shaped HREE zoning throughout grains or, in larger grains, show such zoning around a compositionally homogeneous core (Smit et al., 2013a). For REE from Lu to Nd, the maximum REE concentrations of grain cores decreases, and the width of the compositional core increases, as is typical of Rayleigh distillation (Hollister, 1966; Otamendi et al., 2002). The HREE concentrations are lowest 0.5 mm from grain rims, increasing to rim compositions, which are identical among grains of different size.

## 2.2 | Felsic migmatite *EK2-1*—Western Gneiss Complex, Western Norway

Sample *EK2-1* is from the Western Gneiss Complex (WGC), which exposes the high- to ultrahigh pressure (HP; UHP) continental crust of former Baltica. Most of the

WGC comprises orthogneiss derived from c. 1.6 or 1.0 Ga granite, granodiorite or diorite protoliths. These rocks include discrete bodies of mafic and ultramafic rocks, including gabbro, peridotite, and websterite. Eclogites—some orthopyroxene-bearing (Carswell et al., 2003), others bi-mineralic or more aluminous, containing kyanite or zoisite—occur throughout the WGC and represent the (*U*)*HP* equivalents of gabbro and basalt. The (*U*)*HP* mineral indicators and phase assemblages in these rocks indicate an increasing metamorphic gradient in the WGC from amphibolite facies conditions in the east and southeast to (*U*)*HP* conditions in the west, peaking in three seemingly discrete UHP domains. Well over three decades of chronology have detailed the Caledonian history of the WGC (e.g., Carswell et al., 2003; Corfu et al., 2014; Cutts & Smit, 2018; DesOrmeau et al., 2015; Holder et al., 2015; Kylander-Clark et al., 2007; Terry et al., 2000). The (*U*)*HP* metamorphism occurred during the Scandian orogenic episode (420–400 Ma), when the hyper-extended Baltic margin collided with—and was buried beneath—Laurentia (Carswell et al., 2003; Cutts & Smit, 2018; Griffin & Brueckner, 1980; Kylander-Clark et al., 2007; Mørk & Mearns, 1986). This stage was the culmination of a long (100 Ma) orogenic cycle, in which the Iapetus Ocean between Laurentia and Baltica closed, deforming the margins of the two cratons and intervening terranes (Brueckner & van Roermund, 2004; Hacker & Gans, 2005).

Sample *EK2-1* is from the Vågholm quarry on Fjørtoft Island. The island is located in the Nordøyane-Moldefjord UHP domain, which is among the highest-grade domains in the WGC. Peak *P-T* conditions for this sample were estimated at ~3.3 GPa and 820°C (Terry et al., 2000), consistent with observed coesite and polycrystalline quartz pseudomorphs (Wain, 1997). Zircon and monazite U-(Th)-Pb chronology provided a complex age record, with abundance peaks at 2.8–2.5, 1.5–1.3, and 1.1–0.95 Ga, as well as between 540 and 520 Ma and 460–375 Ma. Among the latter, peaks occur at c. 450, 425, 415, 408, and 395 Ma (Holder et al., 2015; Terry et al., 2000; Tual et al., 2022; Walczak et al., 2019), with the earlier ages commonly recorded by accessory mineral inclusions in garnet. Garnet Lu-Hf chronology on *EK2-1* provided an age of  $422 \pm 2$  Ma (MSWD = 1.3; Tual et al., 2022). This is identical to the age at which zircon and monazite show REE patterns indicative of equilibration with the strongly zoned garnet; it also resembles the Lu-Hf garnet age obtained for an eclogite pod included within the migmatites ( $418 \pm 3$  Ma; unpublished data). In-situ Lu-Hf chronology using LA-ICPMS/MS showed that some grains retain Sveconorwegian (c. 1.04 Ga) relict cores and zones (Simpson et al., 2021; Tamblyn et al., 2021). The rock likely represents a Sveconorwegian granulite that was repeatedly

overprinted and deformed, and ultimately partially molten during a Caledonian orogenic cycle that lasted at least 60 million years. Late-stage melting and deformation is recorded until c. 375 Ma by HREE-poor monazite (Terry et al., 2000; Walczak et al., 2019), which coincides with the approximate timing of cooling below ~500°C in this part of the WGC (Cutts et al., 2019; Root et al., 2005). Cooling rates would have been ~20°C Ma<sup>-1</sup>, assuming that *HT* conditions persisted until 395 Ma (Terry et al., 2000).

Sample *EK2-1* is a layered blastomylonite with foliation-parallel bands of leucosome and melanosome bands alternating on a mm- to cm-scale (Figure 2b). The leucosomes comprise plagioclase and quartz, with minor garnet, kyanite, and biotite, whereas the melanosomes comprise the same assemblage, but with quartz and plagioclase in lower modal abundance. Both types of layers contain accessory zircon, monazite and rutile. Garnet grains throughout the rock are generally 2 mm or less in diameter, but are locally up to 5 cm in leucosomes. Large grains commonly contain exsolved rutile needles in their cores, and are rich in inclusions, especially in their rims. The inclusions comprise biotite, apatite, rutile, quartz, kyanite, zoisite, sulfides, graphite, fluids, and polyminerally assemblages dominated by sanidine, biotite, and quartz. The rims are poikiloblastic, containing abundant inclusions of quartz and minor sanidine, biotite, and sulfides. Garnet typically shows relatively smooth major-element zoning with compositionally different cores and rims separated by smooth compositional changes. The inclusion-rich poikiloblastic rims show patchy irregular zoning and are compositionally distinct from other garnet domains, again separated by smooth zoning transitions (e.g., Tamblyn et al., 2021). Line profiles and maps of REE concentration in garnet grains from the Fjørtoft migmatites show distinct differences in the concentrations and zoning between poikiloblastic and inclusion-poor garnet domains (Tual et al., 2022). Poikiloblastic garnet is typically HREE-poor and shows nebulous zoning with no clear core-rim relationships; these domains are interpreted as having (re-)equilibrated in the presence of melt (Tual et al., 2022). Non-poikiloblastic garnet grains or grain domains preserve concentric zoning that consists of distinct subdomains. Although HREE concentrations are highest in the core, one or more HREE-enriched annuli are typically present (Simpson et al., 2021; Tamblyn et al., 2021; Tual et al., 2022).

### 2.3 | Mafic granulite *SU03A*—Semail Ophiolite (Oman)

Garnet was investigated in a sample from the high-grade upper part of the metamorphic sole of the Semail



Ophiolite, exposed in the Sultanate of Oman and United Arab Emirates. The Semail Ophiolite represents the upper plate of a fossil nascent subduction zone, separated from lower-plate clastic sediments by a series of thrust slices and the Semail Thrust, which accommodated subduction and exhumation of the thrust slices during ophiolite obduction (Searle & Cox, 1999; Searle & Malpas, 1980; Soret et al., 2017). Peak metamorphic conditions across the sole range from  $\sim 500^\circ\text{C}$  and 0.5 GPa to  $\sim 850^\circ\text{C}$  and 0.8 GPa; the increase is discontinuous, marking differences between thrust slices (Searle & Cox, 1999; Soret et al., 2017). The oceanic lithosphere above the Semail Thrust is generally interpreted to have formed in a very short interval between c. 96.3 and 95.5 Ma, as indicated by high-precision U–Pb dating of zircon from gabbros, trondhjemites, and plagiogranites (Rioux et al., 2013). The  $^{40}\text{Ar}/^{39}\text{Ar}$  dates from hornblende in the metamorphic sole exposed at both the Wadi Tayyin and Wadi Sumeini type localities record cooling below  $\sim 525^\circ\text{C}$  at 93–92 Ma, indicating exhumation within a few million years after ophiolite formation (Hacker, 1994). Older ages have long been recognized in Semail, but are typically not interpreted in the context of the burial and exhumation cycle of the ophiolite; c. 112 Ma zircon U–Pb ages from gabbros close to the upper-plate Moho were interpreted to represent xenocrysts, 107–102 Ma zircon U–Pb ages from metapelites from the metamorphic sole were considered as detrital component (Garber et al., 2020, although see Soret et al., 2022), and hornblende  $^{40}\text{Ar}/^{39}\text{Ar}$  ages older than the main cluster at 93–92 Ma were, at least in part, attributed to extraneous  $^{40}\text{Ar}$  (Hacker, 1994; Hacker et al., 1996). Early sole metamorphism was nevertheless indicated by 3 consistent garnet Lu–Hf ages of c. 104 Ma, which were obtained for garnet-clinopyroxene granulite relics in amphibolites from the highest-grade part (c.  $800^\circ\text{C}$ , 1.2 GPa) of the metamorphic sole at Wadi Tayyin and Wadi Sumeini (Guilmette et al., 2018). Garnet from amphibolites in a metasediment-bearing unit within the sole, as well as from clinopyroxene-bearing rocks, yielded younger Lu–Hf ages (c. 96 Ma; Garber et al., 2020, 2023). These ages were taken as a means to scrutinize the geological significance of the older Lu–Hf ages (Garber et al., 2020, 2023). Whether direct comparison is warranted nevertheless is doubtful, given that garnet from the higher-grade sample was significantly resorbed and potentially recrystallized (Garber et al., 2023), and garnet in the amphibolite represents a lower-grade thrust slice that records markedly lower peak  $P$ – $T$  conditions than the granulites (c.  $670^\circ\text{C}$ , 0.8 GPa; Garber et al., 2020); the sole comprises different thrust slices with different histories (Soret et al., 2017). Both titanite U–Pb ages from sole amphibolites and monazite U–Th–Pb ages from

metasedimentary rocks independently confirm an early onset of prograde metamorphism ( $>100$  Ma) and further illustrate that sole metamorphism is not a single-stage process that affected all units at the same time (Soret et al., 2022). Zircon from felsic segregations within mafic granulites record peak- $T$  metamorphism at suprasolidus conditions between 96.2 and 94.5 Ma, whereas titanite U–Pb dating shows that the rocks then exhumed and cooled to  $500^\circ\text{C}$  by 92.6 Ma, consistent with the  $^{40}\text{Ar}/^{39}\text{Ar}$  age from sole hornblende (Guilmette et al., 2018; Hacker et al., 1996). There is no geological evidence for intermittent cooling between garnet growth and the occurrence of suprasolidus conditions, indicating that the sole granulites record a continuous  $P$ – $T$ – $t$  history, involving c. 12 million years of  $HT$  metamorphism followed by exhumation and cooling at an average rate of  $\sim 70^\circ\text{C Ma}^{-1}$ .

Sample *SU-03A* is from Wadi Sumeini and comprises mafic granulite relics in a tectonized hornblende-plagioclase matrix. The relics comprise an assemblage of garnet, diopside and plagioclase, with accessory titanite, ilmenite, apatite, and zircon. The analysed garnet grain is relatively large ( $>1$  mm) and poikiloblastic (Figure 2c; see also fig. 3a of Guilmette et al., 2018). It comprises a high-CaO core containing titanite surrounded by an inclusion-rich mantle in which MgO and FeO increase steadily towards the rims. The mantle contains ilmenite, as well as polyphase inclusions interpreted as former melt inclusions, and is surrounded by a relatively inclusion-poor rim that is compositionally similar to the outermost mantle (Guilmette et al., 2018). Trace-element mapping of the grain showed that the core and mantle are relatively enriched in HREE. The rim exhibits well-developed oscillatory zoning, with HREE concentrations generally increasing towards the grain boundary. The zoning as well as the topology of the mantle-rim and rim-matrix boundaries are similar around the circumference of the entire grain, indicating that the rim developed at a (near-)constant growth rate in all directions away from the core.

## 2.4 | Mafic granulite 6829B3—Shakh dara Dome, Tajikistan

Sample *6829B3* is from the centre of the Shakh dara Dome in the South Pamir, Tajikistan. This dome is the largest in a series of core complexes that developed in the wake of the India–Asia collision (e.g., Hacker et al., 2017; Schmidt et al., 2011; Stearns et al., 2013; Stearns et al., 2015; Stübner et al., 2013, 2013). Prograde metamorphism occurred as a result of collision-induced tectonic thickening, which was underway by c. 44 Ma in

the lower and middle crust of the Shakh dara Dome, and by c. 35–27 Ma in the domes to the north and northeast (Hacker et al., 2017; Smit et al., 2014a; Stearns et al., 2015). The Lu-Hf ages of garnet (41–38 Ma) from lower crustal felsic granulite xenoliths found in ultrapotassic pipes east of the Shakh dara Dome, as well as U-(Th)-Pb ages of zircon and monazite inclusions hosted by xenolith garnet (42–37 Ma; Kooijman et al., 2017) are similar to garnet ages from mafic to felsic granulites of different composition in the Shakh dara Dome (c. 37 Ma; Smit et al., 2014a; Tual et al., 2022). The similarity in the Lu-Hf ages, in spite of differences in rock type, REE zoning, and location (within vs. outside the Shakh dara Dome) indicates rapid synchronous garnet growth across the high-grade part of the South Pamir middle and lower crust. Peak metamorphism in the Shakh dara Dome occurred during the early Miocene (c. 20 Ma) and involved temperatures up to 830°C, as constrained by Zr-in-titanite and Zr-in-rutile thermometry and equilibrium-assembly calculations (Hacker et al., 2017; Smit et al., 2014a; Stearns et al., 2013, 2015). Subsequent exhumation of the Shakh dara Dome rocks occurred by syn-convergent crustal extension, possibly driven by the gravitational collapse of the southwestern margin of overthickened crust of the Pamir plateau (Stübner et al., 2013, 2013). Titanite and rutile U–Pb dating by LA multi-collector ICPMS showed that the Shakh dara granulites remained at high temperature until 14–10 Ma, when they cooled below 600–500°C at an average rate of 30°C Ma<sup>-1</sup> (Smit et al., 2014a; Stearns et al., 2015). Subsequent cooling of rocks in the outcrop of sample 6829B3 is constrained down to 100°C by multi-method thermochronology involving U–Pb titanite dating, <sup>40</sup>Ar/<sup>39</sup>Ar and Rb–Sr biotite dating, and zircon and apatite fission-track dating, and occurred at an average rate of ~55°C Ma<sup>-1</sup> (Smit et al., 2014a; Stearns et al., 2015; Stübner et al., 2013).

Sample 6829B3 (37°08.633'N, 71°44.851'E) is a garnet-, hornblende-, clinopyroxene-, and plagioclase-bearing granulite with a weak foliation and foliation-parallel migmatitic banding (Figure 2d). The matrix between the garnet grains consists of poikiloblastic to symplectitic amphibole and plagioclase with local clinopyroxene remnants. The sample has several leucocratic domains made of plagioclase with mm-scale ilmenite blebs surrounded by thick titanite rims. Garnet grains are sub-euhedral, up to several mm in diameter, and rimmed by amphibole–plagioclase symplectites. The grains contain inclusions of clinopyroxene, amphibole, plagioclase, rutile, and ilmenite. Garnet (alm<sub>54–59</sub>prp<sub>10–18</sub>grs<sub>21–34</sub>sp<sub>0–2</sub>) exhibits smoothly increasing MgO and FeO and decreasing CaO and Mg# towards the rims. Profiles of REE concentrations of garnet in this sample show that grains are concentrically zoned with a HREE-rich core and HREE-

rich annulus at half-radial distance from the core (Smit et al., 2014a; supplement, sample 'SH-3'). The core shows a Rayleigh-fractionation pattern that is often observed for REE in garnet (e.g., Otamendi et al., 2002), with Lu enriched in the core and other REE showing lower maximum concentrations that occur increasingly further away from the compositional core. The HREE-rich annulus shows a repeat of the same systematics, potentially indicating two stages of growth, each limited by REE supply.

### 3 | ANALYTICAL METHODS

#### 3.1 | Trace-element mapping

Trace-element mapping was performed on single grains extracted from the rock (407), on grains in rock fragments (EK2-1, 6829B3), or on grains in thin section (SU-03A). The largest intact grains were selected from each sample. For samples 407, EK2-1, and 6829B3, grains were identified among the processed grain or rock material (407, EK2-1, 6829B3), and mounted as a single grain (407) or garnet-bearing rock fragments (EK2-1, 6829B3) in epoxy. The mounts were then polished down to the geometric core of the target grain. For sample SU-03A, the grain with the largest cross-sectional area similar to that of the largest grains found in the sample was analysed. Given the excessive size of this grain, mapping was restricted to the domain that was previously shown to be zoned for REE. Semi-quantitative trace-element maps of the garnet grains were obtained at the Vegacenter, Swedish Natural History Museum, Stockholm, using an ESI-New Wave NWR193<sup>UC</sup> ArF excimer ( $\lambda = 193$  nm) LA system, equipped with a TwoVol2 two-volume laser cell, coupled to a Nu Instruments Ltd. AttoM HR-ICPMS instrument. Garnet grains were ablated by applying a fluence of 1.5 J cm<sup>-1</sup> at a frequency of 20 Hz to a rectangular (30 × 40 μm) or square (20 × 20 μm) spot, while moving the sample at a velocity of 40 μm s<sup>-1</sup>. The grains were mapped twice and pre-ablated before every pass. In the first pass, the REE concentrations were determined by measuring ion beam intensities at m/z corresponding to <sup>146</sup>Nd, <sup>147</sup>Sm, <sup>153</sup>Eu, <sup>157</sup>Gd, <sup>159</sup>Tb, <sup>163</sup>Dy, <sup>165</sup>Ho, <sup>166</sup>Er, <sup>169</sup>Tm, <sup>172</sup>Yb, and <sup>175</sup>Lu. In the second pass, intensities at m/z corresponding to <sup>45</sup>Sc, <sup>49</sup>Ti, <sup>51</sup>V, and <sup>52</sup>Cr were measured. This double-pass approach enables analysis of all elements in electrostatic deflector mode, which does not require a magnet jump and associated settling time, thus allowing high analytical resolution. Maps from different passes can be directly correlated because ablation depth (~5 μm) is insignificant relative to any down-depth changes in composition. Analytical lines were bracketed by analyses of the NIST 612 reference material. Maps for



all MREE and HREE were completed successfully except for Sm in *EK2-1* and Eu in *EK2-1*, *SU-03A*, and *6829B3*, which suffered ion-counter trips during analysis. Zoning for Sm and Eu in these samples can nevertheless be evaluated through the elemental profiles as provided. The spatially referenced raw intensity data were reduced using *Iolite* (version 4; Paton et al., 2011) employing the *CellSpace* mapping module (Paul et al., 2012). For visualization purposes, inclusions with anomalous elemental concentrations relative to the garnet matrix were filtered out. The maximum concentration of a given REE in a given garnet grain was set as threshold. Where relevant, REE concentrations are normalized to CI chondrite compositions (Boynnton, 1984) and are then marked with a

subscript N. The Eu anomaly ( $\text{Eu}_N/\text{Eu}^*$ ) is  $\text{Eu}_N$  divided by the geometric mean of  $\text{Sm}_N$  and  $\text{Gd}_N$ . All maps and elemental profiles are provided in Figures 3 and 4 (407), 5 (*EK2-1*), 6 (*SU-03A*), and 7 (*6829B3*).

### 3.2 | Numerical modelling of Lu volume diffusion in garnet

Numerical diffusion modelling was done to predict the compositional effects of volume diffusion on the basis of experimentally determined  $D_{\text{HREE}}$ . We investigate Lu, because of its relevance as parent element of the Lu-Hf chronometer. The numerical model solves Fick's second

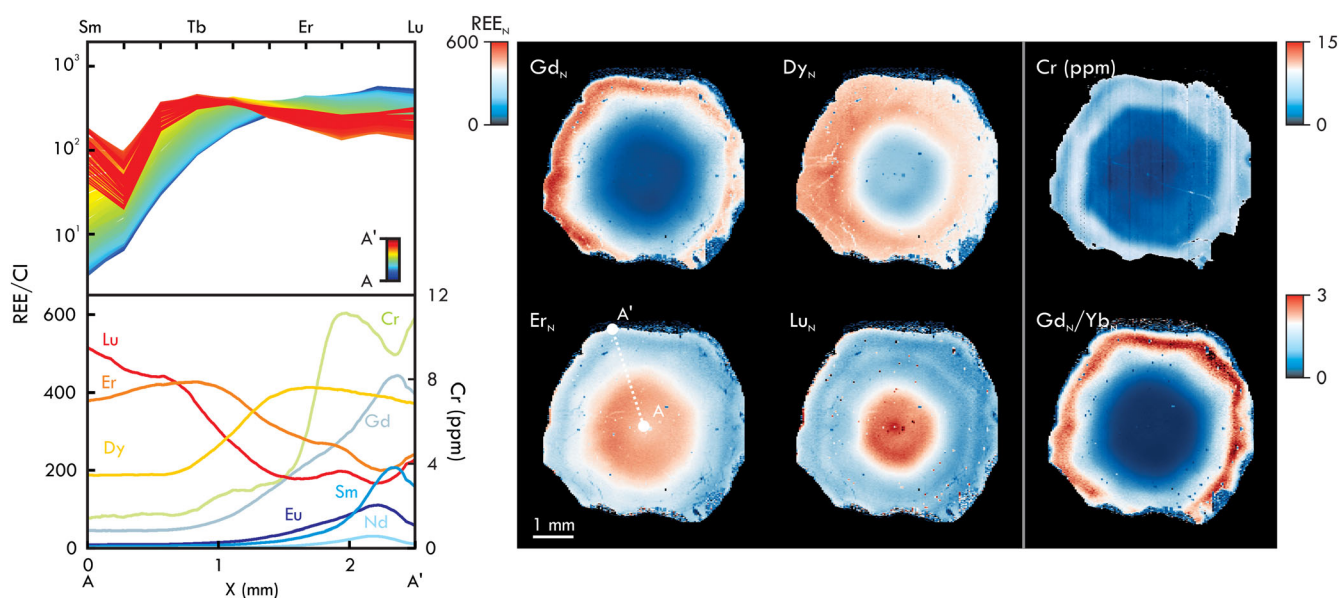


**FIGURE 3** Rare earth elements (REE) and Cr composition and zoning of garnet from Pikwitonei Granulite Domain sample 407. The scale bar for  $\text{REE}_N$  applies to all REE.

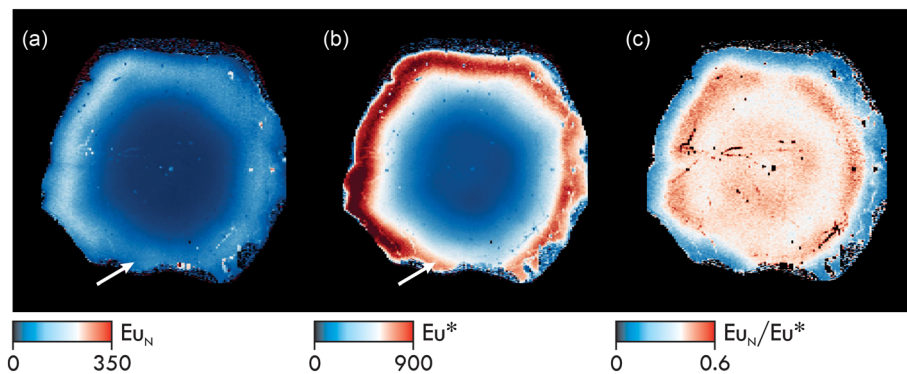


**FIGURE 4** Europium zoning in garnet from samples 407. (a)  $\text{Eu}_N$ , (b)  $\text{Eu}^*$ , that is, the geometric mean of  $\text{Sm}_N$  and  $\text{Gd}_N$ , and (c)  $\text{Eu}_N/\text{Eu}^*$ . The arrow in (a) and (b) shows the promontory where Sm and Gd zoning is preserved, but Eu zoning is largely lost. The maps enable comparison between  $\text{Eu}_N$  as observed (a) and hypothetical  $\text{Eu}_N$ , as it would have been if Eu had not been decoupled from Sm and Gd (b). This comparison shows the controls on the Eu anomaly map shown in (c).

diffusion law for two dimensions using Equation (1), where  $C_{Lu}$  is the concentration of Lu at a given point ( $x$ ,  $y$ ) in the model space and  $D_{Lu}(T)$  is the diffusivity of Lu as a function of temperature ( $T$ ), which is set to decay with the inverse of time.

$$\frac{\partial C_{Lu}}{\partial t} = D_{Lu}(T) \left( \frac{\partial^2 C_{Lu}}{\partial x^2} + \frac{\partial^2 C_{Lu}}{\partial y^2} \right) \quad (1)$$

Simulations were done using  $D_{Lu}(T)$  as estimated for the ‘slow’ and ‘fast’ diffusion mechanisms observed in experiments at 1 atm and 1 GPa, respectively (Bloch et al., 2020). The  $D_{Lu}(T)$  values of these mechanisms differ by about an order of magnitude at the peak temperatures indicated for the different samples. The  $D_{Lu}(T)$  for ‘fast’ diffusion was calculated at given pressure for all samples using the pressure dependence of the activation volume of diffusion as defined by Bloch et al. (2020). The pressure dependence for ‘slow’ diffusion is not defined, but the experimental pressure of 1 GPa is close to the pressures recorded by most samples. For *EK2-1*, a part of high-temperature history occurred at pressure significantly higher than 1.0 GPa (0.8–3.3 GPa; Terry et al., 2000). Assuming an activation volume typical of cation diffusion in garnet (0.6 cm<sup>3</sup>/mol; Ganguly et al., 1998), the activation energy of REE at 800°C would be ~14 kJ higher and  $D_{Lu} \sim 0.5 \log(D_{REE})$  units lower, at 3.3 GPa than at 1 GPa. Assuming 1D diffusion, this lower  $D_{Lu}$  would yield diffusion lengths that are about half that calculated without applying a pressure correction. At least half of the *HT* history of this rock occurred below 2.0 GPa (Terry et al., 2000), which is where pressure effects would be within the experimental uncertainty on  $D_{Lu}$ . The effect of pressure on  $D_{Lu}$  for this sample thus is either minor or insignificant. Pressure conditions for the other samples are within 0.3 GPa of the experimental calibration pressure of 1 GPa. Such differences do not cause significant pressure effects on  $D_{REE}$  of ‘slow’ diffusion.

The modelling focuses on the diffusion that occurred during post-peak cooling, because the duration of peak-*T* conditions, the *P-T* conditions of garnet nucleation, growth, and replacement (in case of *EK2-1*), and the duration of prograde metamorphism are uncertain. Estimated diffusion effects thus provide minimum estimates of the total extent of diffusive re-equilibration. Temperature was set to change according to the cooling rate independently determined for the given terrane. In the absence of detailed time-resolved thermal constraints, cooling rate was kept constant. A first-order pseudo-transient iterative method was used to solve the equations numerically (e.g., Räss et al., 2022), employing a physical time step of 0.01 Ma for all models.

This allowed simulations at high spatial resolution similar to measured trace-element maps while having a constant physical time step for consistency between the models and allowing for sufficiently resolved changes in  $D_{Lu}(T)$ . Initial conditions for the models were based on the Lu concentration maps, assuming that initial compositions showed step-function zoning between local compositional maxima and minima and that all gradual zoning that is now observed between these maxima and minima resulted from diffusive re-equilibration. The initial location of the zoning steps was placed at zoning inflection points, and compositional maxima and minima on either side were taken as the approximate starting compositions. The numerical simulations were performed on the entire garnet grain surrounded by a matrix to allow natural boundary conditions to the modelled space. For simplicity and to establish an end-member scenario for a net change in the Lu budget of garnet, the Lu concentration in the matrix around the garnet is set to zero, such that it acts as an infinite sink for Lu. This boundary condition has no significant bearing on the degree to which volume diffusion is able to erase individual zoning structures in the grain interior and sets no limit to the development of diffusion zoning in the rims. The 2D model provides representations of the *minimum* extent of diffusion that is to be expected for a given grain, because (1) it accounts only for the diffusion *since* peak metamorphism and thus ignores any diffusion that occurred during residence at peak temperature and prograde heating and (2) initial zoning may not have been as sharp as a step-function.

Solving the calculations in 2D was done, because the shape of grains in three dimensions is unknown. The extent of diffusion in 3D may be significantly different from diffusion simulated in the 2D Cartesian numerical model. To quantitatively evaluate this difference, a generic simulation was run in 3D as well, assuming a spherical geometry. For this case, the diffusion equation can be written in radial coordinates, which then essentially becomes a 1D problem (Equation (2); e.g., Lasaga, 1998). Alternatively, the diffusion equation can be expanded to include 3D Cartesian coordinates (Equation (3)).

$$\frac{\partial C_{Lu}}{\partial t} = D_{Lu}(T) \left( \frac{\partial^2 C_{Lu}}{\partial r^2} + \frac{2}{r} \frac{\partial C_{Lu}}{\partial r} \right) \quad (2)$$

$$\frac{\partial C_{Lu}}{\partial t} = D_{Lu}(T) \left( \frac{\partial^2 C_{Lu}}{\partial x^2} + \frac{\partial^2 C_{Lu}}{\partial y^2} + \frac{\partial^2 C_{Lu}}{\partial z^2} \right) \quad (3)$$

The 3D simulation was run by assuming temperature homogeneity and an initial step-function Lu zoning. The

results are shown in Figure 9. The full 3D Cartesian model (Equation (3)) reproduces the 1D spherical model (Equation (2)) reasonably well and this improves when the numerical resolution of the Cartesian model is increased. The 1D Cartesian model yields the least diffused profiles, whereas those of the 2D Cartesian model that was applied to the sample data is intermediate to those provided by the 1D and 3D models. These differences reflect the ability of mass to diffuse in increasingly more dimensions. The difference between the various models largely pertains to the core; towards the rims, diffusion becomes increasingly more unidirectional to the point that model results are identical. This is relevant for the oscillatory zoning observed in some grain rims, where the 2D model should provide a reasonable approximation of diffusive effects. Significant underestimation of these effects are expected for more internal grain domains. This adds to the fact that the model results provide minimum estimates of the extent of diffusion that is to be expected for 'slow' and 'fast' REE diffusion.

## 4 | RESULTS

### 4.1 | Trace element mapping

#### 4.1.1 | Felsic granulite 407—Pikwitonei Granulite Domain (Manitoba, Canada)

The large grain from sample 407 exhibits well-developed REE zoning (Figure 3). The concentrations of REE heavier than Er decrease first gently, then more rapidly towards the rims, only to recover in a slightly HREE-enriched annulus at an  $\sim 2.0$  mm radial distance and in the outermost rim. Zoning of the lighter HREE (e.g., Dy), as well as MREE, is broadly the inverse of those seen in heavier REE. The concentration of these elements increases from a consistent minimum in the core (radial distance: 0 to 1 mm) and decreases again towards the rims. For the MREE, this decrease occurs approximately over the same radial domain as where the HREE concentrations recover. The concentric REE zoning mimics the garnet crystal shape, with well-defined interfacial angles. This is also the case for the slightly HREE-enriched annulus, which also shows relatively sharp corners. The MREE show concentration maxima farther towards the rim with increasing atomic number. Europium (Figure 4) deviates from this trend in several ways: (1) although Eu (Figure 4a) shows a similar pattern as Sm and Gd, its zoning is smoother and interfacial angles are less pronounced (Figure 4b); (2) the maximum Eu concentration is lower than  $\text{Eu}^*$ —the Eu concentration that would be expected on the basis of Sm and Gd if Eu

and these elements had been fully coupled; (3) the maximum Eu concentration occurs further inside the grain than the maximum of  $\text{Eu}^*$  (Figure 4); and (4) In the area where the grain is subhedral (Figures 3 and 4b), Eu zoning is disrupted and more diffuse, and zoning in the remaining promontory of the grain is erased (Figure 4a). This contrasts strongly to Sm and Gd, which still follow the garnet habit all the way to the subhedral grain boundary (Figure 4b). These differences provide the grain with its distinctive high-Eu/ $\text{Eu}^*$  annulus ( $\sim 0.5$ ) and low-Eu/ $\text{Eu}^*$  rims (down to 0.15). Chromium concentrations are low and slightly variable in the inner 2.0 mm radial distance, and increase drastically outward to the rims. This concentric zoning follows the garnet habit closely, similar to the HREE. The maximum Cr concentration occurs at the same radial distance as the HREE-enriched annulus and concentrations decrease slightly at the same radial distance where MREE reach their maximum concentrations. The outer Cr-rich rim appears slightly patchy, but still follows a well-defined concentric relationship to zoning in the inner part of the grain, again with well-defined interfacial angles.

#### 4.1.2 | Felsic migmatite EK2-1—Western Gneiss Complex, Western Norway

The *EK2-1* garnet grain exhibits complex zoning with two distinct domains of different composition (Figure 5). The core of the grain is euhedral and exhibits straight faces joining at sharply defined angles that match the grain-boundary geometry. The Lu concentrations decrease, then increase again within the core. The other HREE (e.g., Er; Figure 5) show less pronounced recovery of concentrations across the core. The MREE zoning is broadly the inverse of the HREE zoning and appears smoother. The HREE-rich core is surrounded by a relatively HREE-poor mantle in which the HREE concentrations gradually decrease and MREE increase. The Eu concentrations are patchy across the core–mantle domain and are slightly higher in the mantle; they lack compositional fluctuations seen in Gd (Figure 5). The mantle is separated from the rim by an irregular interface. The rim is the poikiloblastic part of the grain; it shows patchy zoning for all REE. A nebulous HREE-enriched annulus can be observed at 0.5–1.0 mm radial distance from the grain boundary. The shape of this annulus locally appears to trace the shape of the anhedral grain boundary. Chromium concentrations broadly increase from core to rim, yet the core–mantle–rim relationships as seen in the REE are visible. The Cr zoning within the rim is also nebulous and is broadly the inverse of that observed for the HREE.



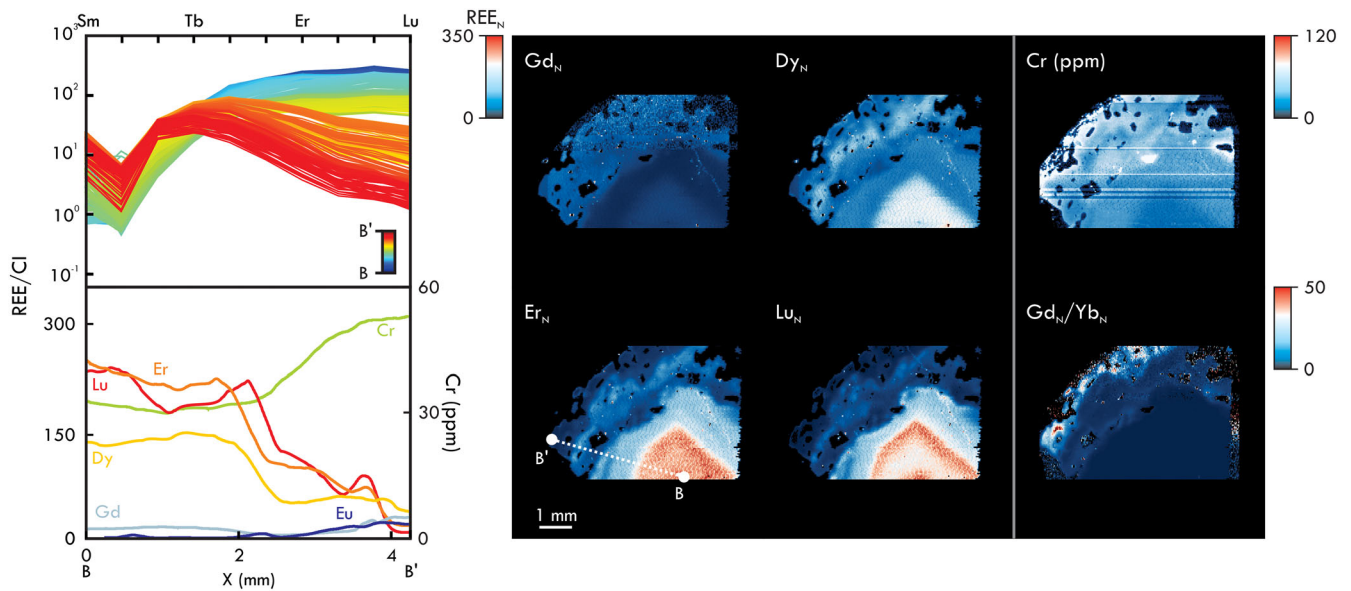


**FIGURE 5** Rare earth elements (REE) and Cr composition and zoning of garnet from Western Gneiss Complex sample *EK2-1*. The scale bar for  $REE_N$  applies to all REE.

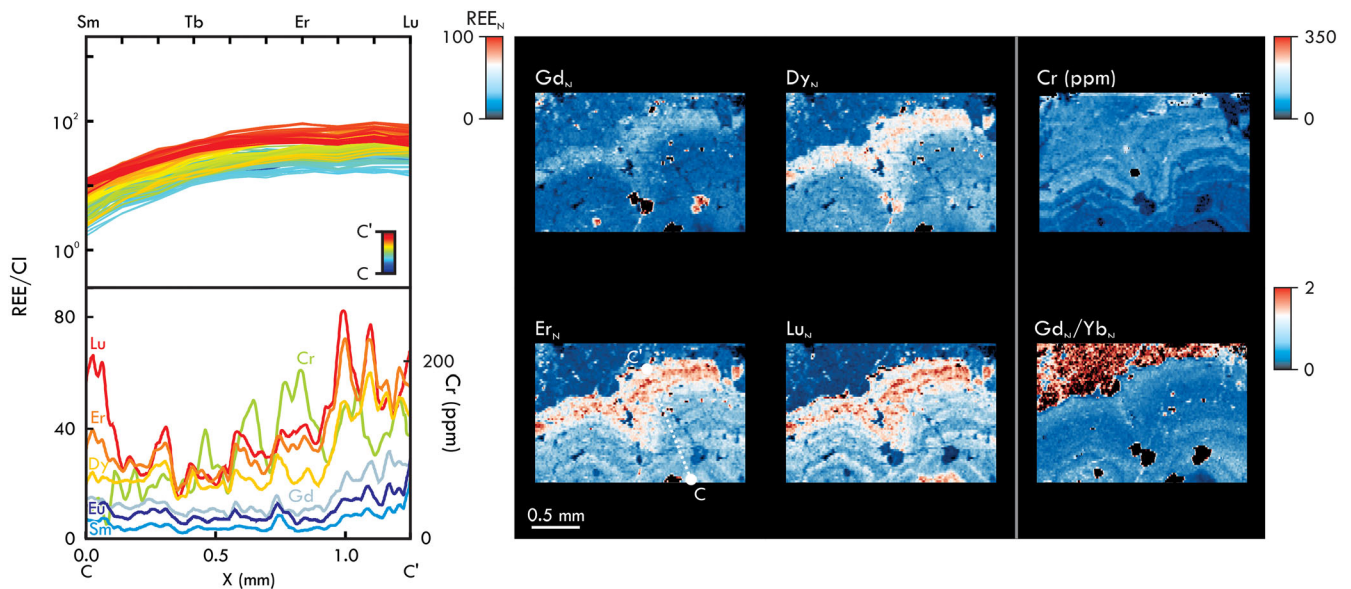


**FIGURE 6** Rare earth elements (REE) and Cr composition and zoning of garnet from Semail Ophiolite sole sample *SU-03A*. The scale bar for  $REE_N$  applies to all REE.

#### 4.1.3 | Mafic granulite SU03A—Semail Ophiolite (Oman)

The mapped domain shows significant oscillatory zoning for all elements analysed (Figure 6). The zoning follows an irregular pattern comprising complex embayments and promontories with sharp angular relationships, which resemble the irregular grain boundary. The innermost part of mapped area shows high HREE and low Cr concentrations and exhibits low Gd/Yb. This part is

surrounded by the oscillatory zoned part of the grain. Across this zone, the oscillations in the concentrations of the HREE and MREE (incl. Eu) are broadly synchronized and broadly correspond to oscillations in Cr concentration. This sets the oscillatory zoning compositionally apart from the internal zone, where HREE zoning is mirrored by that of MREE and Cr. The oscillatory zoned part of the grain can be broadly divided into internal and external domains. In the internal domain, the oscillation wavelength is consistent at  $\sim 0.2$  mm, and the

concentrations of the REE and Cr maxima and minima increase gently outward. In the outer domain, the REE concentration oscillations have a larger amplitude and shorter wavelength, and exhibit higher concentration maxima and minima.

#### 4.1.4 | Mafic granulite 6829B3—Shakh dara Dome, Tajikistan

This mapped grain is the most complex of all grains analysed in this study (Figure 7). The grain can be broadly subdivided into three domains, each with its own REE characteristics. The core is a complex aggregate of inclusions and vein structures, which overprint an otherwise seemingly homogeneous domain. The vein structures locally follow a mesh network connected to small veinlets that emanate outward towards the outer domains and the rim. These veins are highly HREE-enriched. The mantle is less strongly affected by this process and preserves sharp oscillatory zoning with relatively high concentrations of MREE and HREE. Oscillations occur on the scale of 0.1–0.2 mm and are broadly synchronized among all REE as well as Cr. Zones of high concentration show sharply defined interfacial angles and generally mimic the garnet habit, but are not entirely concentric and merge tangentially into adjacent zones. The oscillatory zoned mantle exhibits an outer annulus rich in MREE, Dy and other lighter HREE. The interface between this outer annulus and the rim is sharp, with concentrations changing significantly on the scale of less

than 0.05 mm. This includes Eu, the zoning of which is intermediate to that of Gd and Sm in terms of amplitude and length scale. The rim lacks strong zoning, and is homogeneously enriched in MREE and depleted in HREE.

#### 4.2 | Diffusion modelling

The numerical modelling of the Lu zoning shows that the ‘fast’ diffusion mechanism would cause substantial diffusive rehomogenization in all cases (Figures 8 and 9). For samples 407 and *EK2-1*, sharp corners in concentric zoning patterns are lost within c. 5 Ma, even though temperatures that would sustain further diffusion would be maintained for a substantial period afterwards, especially for sample 407. No trace of oscillatory zoning remains after even 1 Ma in both *SU-03A* and 6829B3. For the ‘slow’ diffusion mechanism, the various characteristic zoning features would persist such that they better resemble those observed in the grains (Figure 8). For all samples except 407, Lu diffusivities for this mechanism are sufficiently low to inhibit further diffusive relaxation after 5 Ma. In 407, this state occurs after c. 100 Ma, by which time zoning is still relatively intact. Although the modelled compositional zoning in *EK2-1* and 407 could arguably match the observations, the oscillatory zoning in garnet from *SU-03A* and 6829B3 is sharper in reality than in the model output. It is thus possible that diffusivity slower than that of the ‘slow’ diffusion mechanism would have provided a better fit between model and reality.

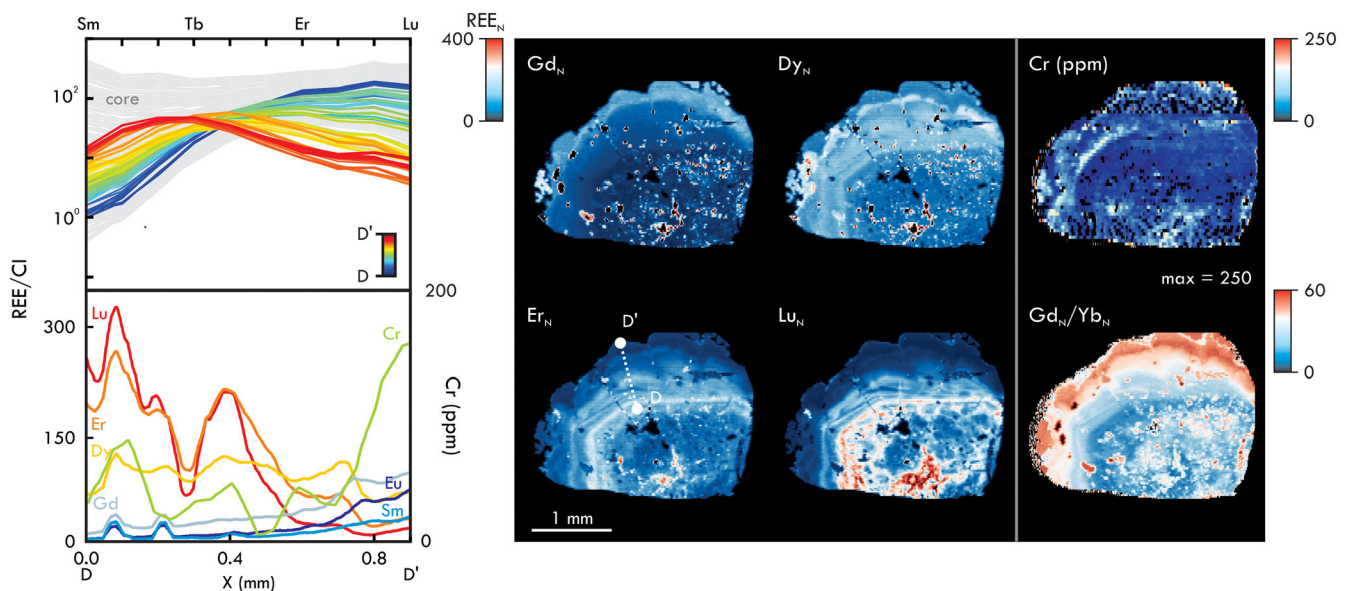


FIGURE 7 Rare earth elements (REE) and Cr composition and zoning of garnet from Shakh dara-Dome sample 6829B3. The scale bar for  $REE_N$  applies to all REE.

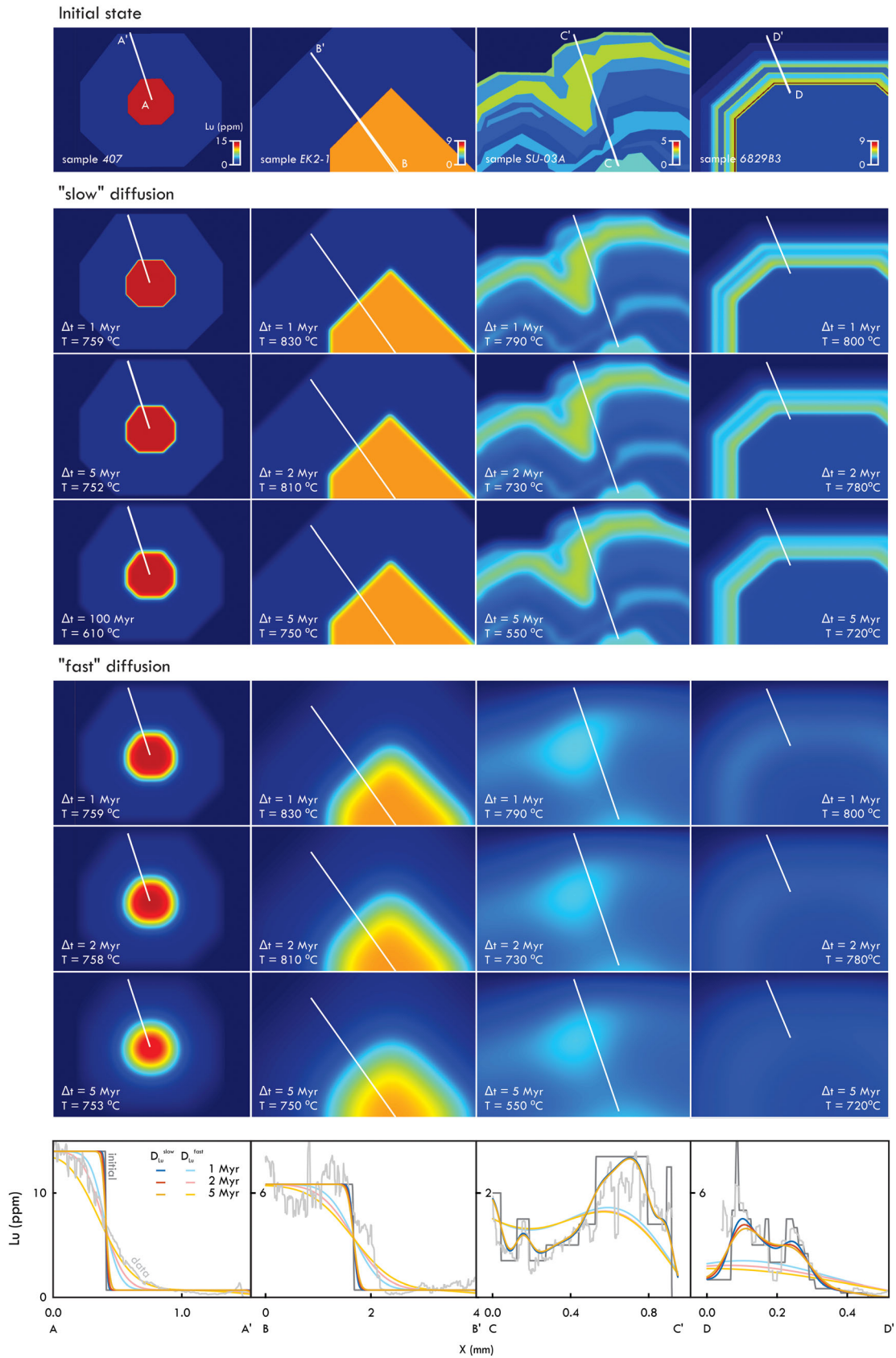


FIGURE 8 Legend on next page.



## 4.3 | Discussion

### 4.3.1 | REE zoning in metamorphosed garnet

A first-order inference from our observations is that garnet in all samples largely, if not entirely, retains REE growth zoning in spite of their extreme thermal histories. The relative retentiveness of REE in garnet is demonstrated by the preservation of strong oscillatory zoning with concentrations changing by almost two orders of magnitude on the scale of tens of micrometres (Figures 5 and 6). Further evidence for REE retentiveness is the fact that changes in the concentration of REE are typically correlated or counter-correlated with changes in the concentration of Cr—an element that diffuses exceedingly slowly in garnet (Carlson, 2012). Another striking feature is the preservation of well-defined interfacial angles in zoning within samples that show more normal bell-shaped HREE zoning (samples *EK2-1* and *407*). The sharp corners in zoning inside the compositional core of *EK2-1* garnet and within the thin HREE-rich annulus in *407* garnet are clear expressions of relict growth zoning that mimics the garnet habit. Numerical modelling (Figure 8) confirms that none of these features should have been preserved if the fast Lu diffusion mechanism that is proposed to occur in garnet below 1 GPa (Bloch et al., 2020) had been active in these grains. Consistent with conclusions from REE diffusion modelling of zoned garnet xenocrysts in granodiorite (Devoir et al., 2021), our numerical diffusion simulations fit the observations better when using the diffusivity as determined for the ‘slow’ diffusion mechanism (Bloch et al., 2020). There are nevertheless indications that Lu diffusion in the natural samples was slower still. The zoning of Lu is sharper than predicted for ‘slow’ diffusion for the samples with preserved oscillatory zoning. This is particularly true considering that (1) the numerical model underestimates the degree of diffusive relaxation (see methods) and (2) the maps likely provide a smoothed version of the actual REE zoning as a result of blurring caused by mixing and aerosol turbulence at the ablation spot size. The observations thus lead to suggest that the diffusion of Lu in natural samples is more sluggish than ‘slow’ diffusion (Bloch et al., 2020) and is likely best represented by the

low diffusivities indicated by natural observations (Carlson, 2012) or the slowest of diffusivities constrained in experiments (van Orman et al., 2002).

The discrepancy between the sluggish diffusion of REE in garnet in nature and the relatively fast diffusion observed in most experiments—‘fast’ diffusion in particular (Bloch et al., 2020)—indicates a fundamental difference in the rate-limiting mechanism. Major-element zoning could be suggested, as compositional contrasts in these elements may cause significant composition-controlled stresses that can work against diffusion (Hess & Ague, 2022). Major-element zoning of garnet in all the samples analysed here, however, is generally smooth, with gradual transitions between zones of different compositions and relatively homogeneous compositions within these zones (see sample description; Smit et al., 2013b, 2014; Guilmette et al., 2018). Alternatively, an explanation may be sought in REE incorporation mechanisms, which control the crystallographic position and diffusive behaviour of REE in garnet (Bloch et al., 2020; Carlson, 2012). In natural silicate garnet, REE are likely incorporated via substitutions involving Na, for example,  $^{\text{VIII}}(\text{REE})^{3+} + ^{\text{VIII}}\text{Na}^{+} \leftrightarrow ^{\text{VIII}}(\text{Ca}, \text{Mn})^{2+}$  and  $^{\text{VIII}}(\text{REE})^{3+} + ^{\text{IV}}(\text{Al}, \text{Fe})^{3+} \leftrightarrow ^{\text{VIII}}(\text{Ca}, \text{Mn})^{2+}$

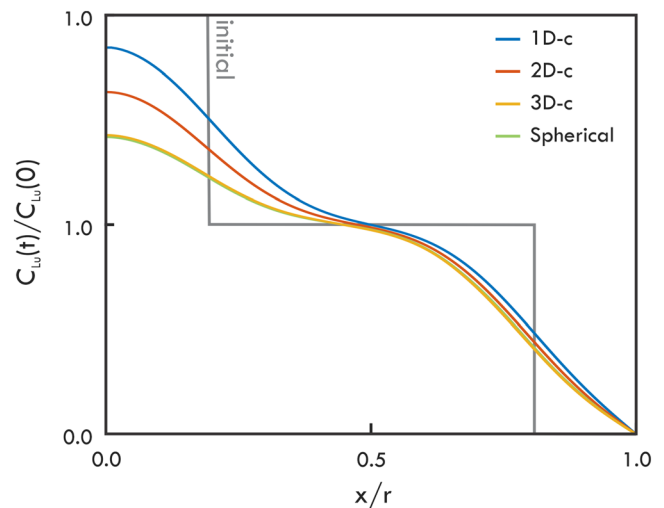


**FIGURE 9** Comparison of results for 1D, 2D, 3D Cartesian (‘c’ marks Cartesian) and spherical diffusion modelling after running the model in non-dimensional time until the initial step functions have been significantly diffused.

**FIGURE 8** Model results for the analysed grains following diffusive relaxation during duration  $\Delta t$ , which is the time elapsed during cooling from peak conditions. Results for ‘slow’ and ‘fast’ diffusion mechanisms (Bloch et al., 2020) are shown. In general, the results are shown up to 5 Ma, because after this period the extent of diffusion is already well beyond the observations (slow diffusion) or diffusivities are no longer sufficient to sustain further compositional change (fast diffusion). The output for 100 Ma is shown for *407* because of its extremely long-lived thermal history. The profiles show initial condition and diffusively relaxed equivalents after 1, 2, and 5 Ma for slow and fast diffusion.

+ <sup>IV</sup>(Si)<sup>4+</sup> (Enami et al., 1995), or via the menzerite substitution <sup>VIII</sup>(REE)<sup>3+</sup> + <sup>VI</sup>(Mg,Fe)<sup>2+</sup> ↔ <sup>VIII</sup>(Mg,Fe)<sup>2+</sup> + <sup>VI</sup>(Al)<sup>3+</sup>. These mechanisms are different from those occurring in experimental diffusion couples, some of which involve the creation of vacancies that—at least in the case of Hf—appear to promote diffusion (Bloch et al., 2020). Diffusion of REE that were incorporated via the menzerite substitution would be exceedingly slow and likely would be equally slow as Cr diffusion, both of which would be rate-limited by the sluggish diffusion of octahedrally coordinated Al (Carlson, 2012). The spatial association of sharp compositional changes in REE and Cr could suggest that these elements indeed are equally retentive. The association is nevertheless not clear enough to represent proper supporting evidence. Although the exact causes for the relatively slow diffusion of REE in natural garnet remain enigmatic, kinetic limitations imposed by sluggish <sup>VI</sup>Al diffusion (Carlson, 2012), with additional limitations caused by major-element zoning (Hess & Ague, 2022), provide the best hypothesis. Diffusion experiments on natural garnet with sharp growth zoning for REE, as well as for Na, Cr, and other minor and trace elements may provide new constraints on this matter.

#### 4.3.2 | Europium versus the other MREE

Where resolvable, zoning in MREE (e.g., Gd; Figures 3–7) preserves interfacial angles (sample 407) and sharp compositional gradients (sample *SU-03A*), indicating MREE zoning is still largely primary and that MREE, like the HREE, have not been significantly affected by diffusive rehomogenization. This inference conforms to experimental observations that suggest that Sm and Yb show equally sluggish diffusion in garnet (van Orman et al., 2002). Europium appears to provide an important exception to this rule. Europium broadly follows the other MREE in the oscillatorily zoned garnet from samples *SU-03A* and *6829B3*. However, in garnet from the slowly cooled sample 407—arguably the sample that underwent the most extreme thermal history of all samples investigated here—there are clear differences in the zoning between Eu and MREE: Eu zoning is smoother and shows less pronounced interfacial angles, Eu shows relatively low maximum concentration and concentration maxima are located more outward in the grain, and zoning following grain shape, rather than grain habit as with Sm and Gd. The result of these differences is a heterogeneous  $\text{Eu}_N/\text{Eu}^*$  that changes from 0.4 in the core to 0.5 in the mantle and down to 0.2 in the rims (Figure 4c). Changes in  $\text{Eu}_N/\text{Eu}^*$  in garnet and various accessory minerals can result from changes in plagioclase stability

and modal abundance, or the extraction or infiltration of melt (Holder et al., 2020; Rubatto, 2002). By this account, the  $\text{Eu}_N/\text{Eu}^*$  zoning in garnet from 407 could be taken to indicate that plagioclase became unstable or that the rock lost melt during the growth of the core and mantle or the garnet, and that plagioclase was stabilized again or that melt infiltrated the rock during growth of the rim. Textural indications for any of these petrological changes are lacking. In fact, plagioclase is a ubiquitous phase in the rock and occurs throughout the matrix, as well as throughout the garnet inclusion assemblage, and the rock has not undergone extensive partial melting as indicated by the abundance and euhedral appearance of biotite. Controls other than mineral assemblage thus must be explored to explain the observed Eu zoning in this sample. The differences listed above are considered consistent with the effects of the diffusive relaxation of primary Eu zoning relative to the zoning of Sm and Gd, and the resulting in-diffusion of Eu towards the core and diffusive loss of Eu to the matrix. Diffusive relaxation of Eu may be attributed to Eu occurring, at least in part, as the more mobile  $\text{Eu}^{2+}$ . The diffusive behaviour of this species likely resembles that of Ca, given that both have a similar valence and ionic radius (Shannon, 1976). Consistent with this expectation, the apparent diffusion length scale for Eu—estimated from the radial distance between the elevated Eu annulus and the rim—is ~0.35 mm, which is identical to the diffusion length scale of Ca (Smit et al., 2013b). Europium thus likely diffuses at similar rates as Ca and can be diffusively decoupled from other MREE during (*U*)HT metamorphism.

It is not entirely clear whether Eu in 407 garnet was incorporated as  $\text{Eu}^{2+}$ , or whether it was incorporated as  $\text{Eu}^{3+}$  and subsequently reduced. The latter, nevertheless, may be most plausible. If Eu had initially been  $\text{Eu}^{2+}$ , it would have been incorporated along with Ca as part of a grandite component. The distribution of Ca in this particular grain is nevertheless distinct from that of Eu; Ca shows no zoning, except for the outermost rim where it decreases in concentration (Smit et al., 2013b), and Ca lacks the rimward increase as seen in Eu concentrations. Although seemingly slightly modified, the zoning in Eu still generally resembles that of Sm and Gd, both of which show a rimward concentration increase as well (Figures 2 and 3). The latter indicates that Eu was predominantly incorporated as  $\text{Eu}^{3+}$  and initially developed zoning similar to that of Sm and Gd, but was later reduced to the more mobile  $\text{Eu}^{2+}$ . The example of garnet in sample 407 indicates that zoning in  $\text{Eu}_N/\text{Eu}^*$  in garnet that has undergone (*U*)HT metamorphism need not record mineral reactions involving plagioclase and may instead result from changes in redox conditions since garnet growth.

### 4.3.3 | Causes of different types of REE zoning

The zoning observed for REE is far more complex than that of major elements and, as a result, provides significantly more insight into the mode of garnet growth and the processes involved in recrystallization. To investigate these aspects for the analysed samples, we evaluated various types of zoning—smooth and concentric, nebulous, and oscillatory—as well as specific REE signatures, for example, Gd/Yb and  $\text{Eu}_N/\text{Eu}^*$ . Garnet with smooth concentric zoning, as seen in *407* and *EK2-1*, shows a rimward decrease in the HREE and increase in the MREE and Cr, often with a second maximum or inflection point for the HREE concentrations halfway along the profile. This normal garnet zoning reflects the common record of Rayleigh fractionation during prograde fractional growth as commonly seen in garnet, with rapid uptake, and depletion and intermittent supply recovery for the garnet-compatible HREE in the effective matrix, and steady accumulation of the less-compatible MREE at the boundary of the growing grain (Konrad-Schmolke et al., 2022; Otamendi et al., 2002; Skora et al., 2006). Consistent with Rayleigh fractionation, Cr shows similar zoning to that of the MREE in these samples, which is consistent with these elements being similarly compatible in garnet (Hauri et al., 1994).

Two samples show poikiloblastic garnet zones with nebulous, patchy or otherwise extremely irregular REE zoning. Textural evidence indicates that such zones are the product of interface-coupled replacement reactions, which is a known mechanism for removing or modifying growth zoning for REE, as well as other elements, for example, P (Ague & Axler, 2016). In sample *EK2-1*, interface-coupled reactions led to the production of a poikiloblastic rim with nebulous REE zoning that is apparently primary as it is equally present in Cr. The zoning of the internal part of the grain is truncated at the boundary with the nebulous rim, clearly reflecting dissolution of the core along a reaction front. Such rims are common in garnet in this sample and linked to migmatization (Tual et al., 2022), indicating that melts likely mediated the interface-coupled replacement process. In sample *6829B3* (Figure 7), the compositional core is likewise poikiloblastic and patchy, and shows a chaotic texture that is unlikely to be primary. The core is connected to the matrix of the grain via veinlets that appear to have enabled the infiltration of reactive fluids or melts from the matrix into the core domain, where they facilitated the replacement of the primary core by patchy, porous garnet.

Oscillatory zoning with oscillations on the scale of 100  $\mu\text{m}$  or less occurs in the two mafic granulites

investigated in this study (Figures 6 and 7). In both cases, the zoning is observed in grain rims around cores that lack such zoning. An explanation for this may be sought in element-transport kinetics and reaction overstepping, and the multi-mode style of growth that occurs as a result (Wilbur & Ague, 2006). The nucleation of garnet is typically significantly overstepped (Wilbur & Ague, 2006; Pattison et al., 2011; Spear, 2017). Upon nucleation, the excess chemical energy of the system causes rapid, voluminous growth of garnet, which will push the system into a supply-limited regime, causing Rayleigh fractionation of the matrix and the development of normal bell-shaped REE zoning. This initial growth spurt depletes the matrix in divalent cation constituents on the rock-scale, decreasing the affinity of the system for renewed garnet growth (Spear, 2017). Renewed growth in energy-depleted matrices will produce volumetrically minor amounts of garnet and such garnet would lack Rayleigh-type zoning owing to crystallization being controlled by growth kinetics rather than element supply. In such a scenario, energy dissipation during epitaxial growth of one garnet zone onto another will form garnet with compositional oscillations that have a predictable and consistent wavelength, even at constant  $P$ – $T$ – $X$  (Jamtveit, 1991). Such process would predict co-variation of garnet-compatible elements within individual growth annuli, as is seen for the REE in the rims of garnet in both *6829B3* and *SU-03A*. The above model of two-stage kinetics-controlled growth to explain normally zoned garnet cores with oscillatory zoned rims may be validated by observations from garnet formed in skarns. Such garnet also commonly shows oscillatory zoning as a reflection of energy dissipation during growth, but such zoning is typically observed throughout grains rather than just in rims (Baxter et al., 2017; Jamtveit, 1991; Park et al., 2017). This difference may be attributed to the fact that garnet nucleation in skarns is not strongly overstepped and reaction affinity is budgeted more evenly throughout the growth history.

Oscillatory zoning has been observed for various elements in garnet from a variety of metamorphic rocks, for example, amphibolite facies metapelites (Gaidies et al., 2021; George et al., 2018; Kohn, 2004; Moore et al., 2013; Schumacher et al., 1999; Stowell et al., 2011), and blueschists, eclogites, and amphibolites exhumed from subduction zones (Angiboust et al., 2014; Garcia-Casco et al., 2002; Konrad-Schmolke et al., 2022; Moore et al., 2013; Rubatto et al., 2020; Tsujimori et al., 2006; Viète et al., 2018). Much like in garnet from samples *SU-03A* and *6829B3*, oscillatory zoning in each of these cases occurs exclusively in external domains—in grain rims or, in the case of garnet from Nepalese metapelites, as an outermost zone of grain cores. The oscillatory zoning in



these cases is typically ascribed to imposed mechanisms, for example, pulsed mineral reactions, changes in matrix permeability, rapid switches between open and closed-system fluid-flow, cyclic over-pressurization, and rapidly changing  $P$ - $T$  conditions due to pulses of thrust-loading, tectonic burial, heating, or exhumation. Open-system behaviour to form oscillatory zoning can be tested using stable isotopes (e.g., Hoover et al., 2022), but the other imposed mechanisms may be difficult to test. In absence of direct supporting evidence for these, kinetic effects such as those described above may be considered to explain the common textural association of oscillatory zoned rims around compositionally distinct cores in garnet within metamorphic rocks.

#### 4.3.4 | Implications for garnet Lu-Hf chronology

The retentiveness of REE indicated by our observations has significant implications for garnet chronology, where the role of REE diffusion is long-contended. Diffusive exchange of REE between garnet and matrix at very high temperatures may affect garnet Lu-Hf and Sm-Nd age systematics in different ways (e.g., Baxter et al., 2017; Baxter & Scherer, 2013; Bloch et al., 2020; Mezger et al., 1992; Scherer et al., 2000; Smit et al., 2013a). For the Sm-Nd system, where the diffusivity of parent and daughter elements is similar, this process can lead to garnet dates that partially or entirely represent cooling (e.g., Anczkiewicz et al., 2007; Johnson et al., 2018; Smit et al., 2013a). For the Lu-Hf system, the higher diffusivity of the parent element (Lu) in garnet relative to that of the daughter element (Hf) potentially results in complex behaviour. In early studies using combined Lu-Hf and Sm-Nd geochronology on slowly cooled samples that were not adversely affected by inclusions, Lu-Hf dates were somewhat older than Sm-Nd ages for the same material, indicating that closure temperatures of Lu-Hf in garnet were greater than or equal to those of Sm-Nd (Scherer et al., 2000). This was seemingly at odds with the observation that Lu diffuses faster than Sm and Nd (e.g., Ganguly et al., 1998; Ganguly & Tirone, 1999), which led to suggest that Lu controls the closure systematics of the Lu-Hf system in garnet (Ganguly & Tirone, 1999). The reincorporation of Lu during partial resorption, presumably by volume diffusion, can indeed perturb Lu-Hf age systematics. An illustrative example of this is provided by thermally overprinted garnet from the contact-metamorphic aureole of the Makhavinekh Lake Pluton, Labrador, where garnet resorption and preferential Lu re-uptake during a thermal overprint caused garnet Lu-Hf ages trailing down from the crystallization

age to the age of the overprint (Kelly et al., 2011). A similar effect may be seen in garnet in a migmatitic gneiss from the Kangchenjunga Himal, which is strongly resorbed and exhibits nebulous rims enriched in Lu, and yielded a Lu-Hf age that is significantly younger than those of other samples from the same area (Lihter et al., 2022). Views diverge on whether Lu diffusion could influence chronometer systematics of garnet that was not affected by resorption and Lu re-uptake during a much-younger metamorphic overprint. In general, the Lu concentration in dated minerals and their matrix are held essentially constant by partitioning behaviour at temperatures where diffusion operates on a significant scale, which would imply that the Lu budget of the garnet reservoir is effectively fixed, regardless of whether Lu had diffused, and that the diffusion of Hf thus should govern Lu-Hf age systematics (Baxter & Scherer, 2013; Scherer et al., 2000; Smit et al., 2013a). Relaxation of growth zoning in garnet porphyroblasts through volume diffusion was nevertheless shown to potentially cause an increase in Lu concentration at garnet rims, which could cause some degree of Lu loss to the matrix (e.g., Kohn, 2009) even if garnet-matrix partition coefficients were to stay constant. If significant accumulation of radiogenic  $^{176}\text{Lu}$  in garnet had occurred before this Lu loss, the latter process could cause garnet-matrix Lu-Hf isochrons to have excess scatter (Kohn, 2009) and to provide spuriously old ages (Bloch & Ganguly, 2015; Kohn, 2009). Changes in partition coefficients with temperature may factor into this as well (Bloch & Ganguly, 2015), which leads to suggest that Lu-Hf ages that are made spurious by Lu diffusion may be significantly older or younger than the growth age depending on bulk-rock composition and mineral assemblage. Whether the  $^{176}\text{Lu}/^{177}\text{Hf}$  of garnet and matrix can actually be modified by Lu diffusion during single metamorphic cycles hinges on whether Lu diffusion is as fast in natural garnet as it is in experiments, which the present study shows not to be the case; the diffusivity of Lu as determined in experiments would not have allowed the preservation of the Lu zoning observed in the present study. From this follows that there is a significant risk for misinterpretation when using experimentally determined Lu diffusivities—especially those for the ‘fast’ mechanism—in Lu-Hf age interpretation, Lu diffusion modelling, and REE-based speedometry; the constraints on ‘slow’ diffusion may provide more realistic results, but even these may overestimate the extent of Lu diffusion.

The findings from the REE maps obtained in this study stimulate a critical assessment of various examples where results from numerical modelling using experimental  $D_{\text{Lu}}$  were used to (re-)interpret Lu-Hf data. One such case pertains to a Lu-Hf age from a migmatitic

schist in the Putomayo Orogen, *S. Columbia* (Ibañez-Mejia et al., 2018). The Lu-Hf age for garnet in this rock ( $1071 \pm 6$  Ma) is older than the U-Pb ages from metamorphic zircon in nearby rocks (1050–980 Ma) and is also older than the expected garnet growth age of 1,060 Ma, which was calculated on the basis of a single-stage thermal evolution constrained by an apparent Sm-Nd cooling age (c. 1007 Ma). An explanation of this Lu-Hf age was argued to ‘require preferential retention of  $^{176}\text{Hf}/^{177}\text{Hf}$  and thus isochron skewing by diffusive Lu loss from garnet (Bloch et al., 2020). However, even when assuming that the apparent age difference of 5–10 Ma (0.5–1%) is significant, such difference could just as easily be explained as reflecting a robust chronometer dating garnet formation as one of the earliest metamorphic processes in the history of this rock. Whereas cases that arguably show Lu-Hf isochron skewing are inconclusive, the same cannot be said for cases of (*U*)*HT* rocks where such effect can be ruled out. For example, Lu-Hf garnet ages from the Shakh dara Dome (peak  $T = 830^\circ\text{C}$ ;  $dT/dt = 20 \text{ K Ma}^{-1}$ ) are identical at c. 37 Ma (within 0.3–1.2 Ma uncertainty, 2 SD), regardless of significant differences in bulk rock composition (mafic vs. felsic) and garnet grain size (0.5 vs. 4 mm radius), and this age matches a cluster of U-Pb ages from prograde titanite within the same terrane (Smit et al., 2014a; Stearns et al., 2015). The Lu-Hf ages of garnet from the Mistinibi-Raude Domain, SE Churchill Province, precisely date the onset of a c. 70 million year *HT* history (peak  $T$  at  $\sim 800^\circ\text{C}$ ) and match the ages of metamorphic monazite, in spite of garnet grains being extremely poikiloblastic and effectively fine-grained (Godet et al., 2020). Garnet porphyroblasts in the Sikkim Himalaya, which were metamorphosed at  $\sim 800^\circ\text{C}$ , provide age- $T$  data that match the trend observed for lower-grade rocks in the same Barrovian sequence (Anczkiewicz et al., 2014), which would not be the case had they become spurious. Fine-grained garnet (<0.5 mm) in mafic and felsic granulites from the Orlica-Śnieżnik Dome (Bohemian Massif) underwent c. 10 million years of *HT* metamorphism with a peak  $T$  of  $\sim 950^\circ\text{C}$ , yet yielded Lu-Hf ages that match the U-Pb age of metamorphic zircon rims, which were interpreted to have co-crystallized with garnet on the basis of REE signatures (Walczak et al., 2017). The observations made in this study provide context as to why the Lu-Hf system is so robust and why predicted effects of Lu diffusion are not reflected in these cases.

Implications of the Lu retentiveness observed in this study also pertain to the interpretation of the Lu-Hf ages that were obtained for sample 407 and were used to empirically constrain the closure-temperature systematics of the Lu-Hf system in garnet (Smit et al., 2013a). The ages (2.71–2.64 Ga) were originally interpreted as

reflecting single-stage garnet nucleation and growth at 2.71 Ga with subsequent younging in smaller grains caused by diffusive loss of radiogenic Hf. This interpretation takes into account that (1) the grains show similar REE zoning across the grain size range, thus indicating that the grains are cogenetic, yet grew to different sizes, (2) the apparent Lu-Hf ages broadly correlate with grain size, not with REE zoning, and (3) the 2.71 Ga age matches the onset of ‘M1’—the earliest regional metamorphism in the area (Mezger et al., 1989a; Heaman et al., 2011)—and is identical to the  $^{207}\text{Pb}/^{206}\text{Pb}$  ages of inclusions in garnet from felsic segregations in nearby mafic rocks (Mezger et al., 1989a). In spite of this, the ages were considered spurious and were instead reinterpreted as recording long-lived growth, starting at 2.73 Ga and ending at 2.66 Ga (Bloch et al., 2020; Bloch & Ganguly, 2015). The interpretation that Lu concentrations of garnet had been unaffected by diffusive exchange (Smit et al., 2013a) was furthermore called into question given latest diffusion parameters (Bloch et al., 2020). These aspects, along with theoretical considerations, were considered sufficient basis for questioning the empirical constraints on the closure systematics of the Lu-Hf chronometer (Bloch et al., 2020). However, this reinterpretation puts garnet growth well before the onset of the first metamorphism in the area (Heaman et al., 2011) and would imply continuous garnet growth over more than 60 Ma, which is geologically unlikely considering that metamorphism in the PGD occurred in discrete pulses (Heaman et al., 2011). The modelled age-grain size relationship that was obtained using this reinterpretation (Bloch et al., 2015) speaks neither for nor against the validity of the results. In fact, what is noted to demonstrate ‘excellent agreement between the simulated and measured  $^{176}\text{Lu}$ – $^{176}\text{Hf}$  [...] garnet ages’ (Bloch et al., 2015) is in reality a model result that is doubtful given the unrealistic thermal and garnet-growth history and falls in the range of data that are too imprecise and too poorly correlated to allow a robust positive test. The interpretation that it is typically Hf, not Lu, that controls Lu-Hf age systematics (Scherer et al., 2000) may also not be as ‘demonstrably inaccurate’ as suggested (Bloch et al., 2020). Garnet resorption and diffusive Lu reuptake during much later overprinting may affect Lu-Hf age signatures (e.g., Kelly et al., 2011; Lihter et al., 2022). However, in any case where such process did not occur, partitioning behaviour (Scherer et al., 2000) and sluggish Lu diffusion will cause the concentrations of Lu in the garnet and matrix to be held approximately constant over the cooling interval between Hf and Lu closure, thus leaving diffusive Hf exchange between garnet and matrix as the only mechanism by which Lu-Hf ages can be significantly changed. This leaves a few theoretical objections

against the original data treatment (Bloch et al., 2020). These, however, do not diminish the validity of the basic conclusion of the original study: the Lu-Hf system in garnet is highly robust against thermal disturbance and permits reliable dating of garnet growth and recrystallization in the crust, even in cases where (*U*)*HT* overprinting has occurred. This conclusion is supported by the fact that a clear and convincing case of a crustal garnet, where the Lu-Hf age system was affected by the diffusion of either Lu or Hf, has not been found yet. The conclusion has special bearing on the common case, where Lu-Hf ages are older than ages obtained from accessory minerals from the same rock or area (Figure 1a). Rather than indicating spuriousness (e.g., Bloch et al., 2020; Garber et al., 2023), such old Lu-Hf ages more likely provide valuable and often unique age constraints on the prograde metamorphism, which can pinpoint tectonic and geodynamic events that are key to the development of orogens and (super-)continents (e.g., Johnson et al., 2018; Pourteau et al., 2018).

#### 4.4 | Synthesis

The results from trace-element mapping and numerical diffusion modelling in this study demonstrate that the REE diffuse exceedingly slowly in natural garnet—slower than expected on the basis of recent diffusion experiments and slow enough to prevent significant changes to REE zoning, even in cases where garnet underwent protracted or repeated *HT* overprinting. Even though Lu likely still diffuses faster than Hf, Lu diffusion will—in the vast majority of cases—be unable to significantly affect Lu contents and Lu/Hf, and, by extension, Lu-Hf ages of garnet. This validates the qualitative assessment that the systematics of the Lu-Hf chronometer in garnet is controlled by the daughter element Hf (Baxter & Scherer, 2013; Scherer et al., 2000). Trace-element mapping provides a new avenue for testing the diffusive behaviour of Lu in other minerals used in the Lu-Hf chronology of terrestrial and planetary materials, and for investigating complex mineral reaction and growth mechanisms that may not—or may no longer—be reflected in major element compositions. This approach thus provides an essential new tool for the empirical testing of solid-state mass transfer in and among metamorphic minerals.

#### ACKNOWLEDGEMENTS

We acknowledge A. Karlsson for assistance with sample preparation and for useful discussions. Constructive comments and suggestions from J.J. Ague and M. Konrad-Schmolke greatly helped improve the manuscript, and

editorial handling by S. Penniston-Dorland is gratefully acknowledged. Funding was provided by the Natural Sciences and Engineering Research Council of Canada (Discovery Grant RGPIN-2020-04692 and Accelerator Grant RGPAS-2020-00069 to M. A. S.), the Swedish Research Council (National Infrastructure Grant 2017-00671 to E. K. and International Postdoc grant 2018-00200 to L. T.) and the European Union's Horizon 2020 research and innovation programme (Marie Skłodowska-Curie grant 899546 to L. T.). J. C. V. has been partially funded by Deutsche Forschungsgemeinschaft (Project Number 235221301/C09). This is Vegacenter contribution #073.

#### ORCID

Carl Guilmette  <https://orcid.org/0000-0001-7196-522X>

#### REFERENCES

- Ague, J. J., & Axler, J. A. (2016). Interface coupled dissolution-reprecipitation in garnet from subducted granulites and ultrahigh-pressure rocks revealed by phosphorous, sodium, and titanium zonation. *American Mineralogist*, *101*, 1696–1699. <https://doi.org/10.2138/am-2016-5707>
- Anczkiewicz, R., Chakraborty, S., Dasgupta, S., Mukhopadhyay, D., & Koltonik, K. Timing, duration and inversion of prograde Barrovian metamorphism constrained by high resolution Lu–Hf garnet dating: A case study from the Sikkim Himalaya, NE India, earth planet. *Science Letters*, *407*, 70–81. <https://doi.org/10.1016/j.epsl.2014.09.035>
- Anczkiewicz, R., Szczepański, J., Mazur, S., Storey, C., Crowley, Q., Villa, I. M., Thirlwall, M. F., & Jeffries, T. E. (2007). Lu–Hf geochronology and trace element distribution in garnet: Implications for uplift and exhumation of ultra-high pressure granulites in the Sudetes, SW Poland. *Lithos*, *95*, 363–380. <https://doi.org/10.1016/j.lithos.2006.09.001>
- Angiboust, S., Pettke, T., De Hoog, J. C. M., Caron, B., & Oncken, O. (2014). Channelized fluid flow and eclogite-facies metasomatism along the subduction shear zone. *Journal of Petrology*, *55*, 883–916. <https://doi.org/10.1093/petrology/egu010>
- Baxter, E. F., Caddick, M. J., & Dragovic, B. (2017). Garnet: A rock-forming mineral petrochronometer. *Reviews in Mineralogy and Geochemistry*, *83*, 469–533. <https://doi.org/10.2138/rmg.2017.83.15>
- Baxter, E. F., & Scherer, E. E. (2013). Garnet geochronology: Time-keeper of tectonometamorphic processes. *Elements*, *9*, 433–438. <https://doi.org/10.2113/gselements.9.6.433>
- Bloch, E., & Ganguly, J. (2015). <sup>176</sup>Lu–<sup>176</sup>Hf geochronology of garnet II: Numerical simulations of the development of garnet-whole-rock <sup>176</sup>Lu–<sup>176</sup>Hf isochrons and a new method for constraining the thermal history of metamorphic rocks. *Contributions to Mineralogy and Petrology*, *169*(2015), 14. <https://doi.org/10.1007/s00410-015-1115-x>
- Bloch, E., Ganguly, J., Hervig, R., & Cheng, W. (2015). <sup>176</sup>Lu–<sup>176</sup>Hf geochronology of garnet I: Experimental determination of the diffusion kinetics of Lu<sup>3+</sup> and Hf<sup>4+</sup> in garnet, closure temperatures and geochronological implications. *Contributions to Mineralogy and Petrology*, *169*, 12. <https://doi.org/10.1007/s00410-015-1109-8>



- Bloch, E., Jollands, M. C., Devoir, A., Bouvier, A.-S., Ibañez-Mejía, M., & Baumgartner, L. P. (2020). Multispecies diffusion of yttrium, rare earth elements and hafnium in garnet. *Journal of Petrology*, *61*, ega055. <https://doi.org/10.1093/petrology/egaa055>
- Boynton, W. V. (1984). Cosmochemistry of the rare earth elements: meteorite studies. In P. Henderson (Ed.), *Developments in geochemistry* (pp. 63–114). Elsevier. <https://doi.org/10.1016/B978-0-444-42148-7.50008-3>
- Brueckner, H. K., & van Roermund, H. L. M. (2004). Dunk tectonics: A multiple subduction/duction model for the evolution of the Scandinavian Caledonides. *Tectonics*, *23*, TC2004. <https://doi.org/10.1029/2003TC001502>
- Carlson, W. D. (2012). Rates and mechanism of Y, REE, and Cr diffusion in garnet. *American Mineralogist*, *97*, 1598–1618. <https://doi.org/10.2138/am.2012.4108>
- Carswell, D. A., Brueckner, H. K., Cuthbert, S. J., Mehta, K., & O'Brien, P. J. (2003). The timing of stabilisation and the exhumation rate for ultra-high pressure rocks in the Western gneiss region of Norway. *Journal of Metamorphic Geology*, *21*, 601–612. <https://doi.org/10.1046/j.1525-1314.2003.00467.x>
- Corfu, F., Austrheim, H., & Ganzhorn, A.-C. (2014). Localized granulite and eclogite facies metamorphism at Flatraket and Kråkeneset, Western gneiss region: U–Pb data and tectonic implications. *Special Publication. Geological Society of London*, *390*, 425–442. <https://doi.org/10.1144/SP390.22>
- Cutts, J. A., & Smit, M. A. (2018). Rates of deep continental burial from Lu–Hf garnet chronology and Zr-in-rutile thermometry on (ultra)high-pressure rocks. *Tectonics*, *37*, 71–88. <https://doi.org/10.1002/2017TC004723>
- Cutts, J. A., Smit, M. A., Kooijman, E., & Schmitt, M. (2019). Two-stage cooling and exhumation of deeply subducted continents. *Tectonics*, *38*, 863–877. <https://doi.org/10.1029/2018TC005292>
- Cutts, J. A., Smit, M. A., & Vrijmoed, J. C. (2020). Evidence for non-lithostatic pressure in subducted continental crust. *Contributions to Mineralogy and Petrology*, *175*, 3. <https://doi.org/10.1007/s00410-019-1633-z>
- DesOrmeau, J. D., Gordon, S. M., Kylander-Clark, A. R. C., Hacker, B. R., Bowring, S. A., Schoene, B., & Samperton, K. M. (2015). Insights into (U)HP metamorphism of the Western gneiss region, Norway: A high-spatial resolution and high-precision zircon study. *Chemical Geology*, *414*, 138–155. <https://doi.org/10.1016/j.chemgeo.2015.08.004>
- Devoir, A., Bloch, E., & Müntener, O. (2021). Residence time of igneous garnet in Si-rich magmatic systems: Insights from diffusion modeling of major and trace elements. *Earth and Planetary Science Letters*, *560*, 116771. <https://doi.org/10.1016/j.epsl.2021.116771>
- Enami, M., Cong, B., Yoshida, T., & Kawabe, I. (1995). A mechanism for Na incorporation in garnet: An example from garnet in orthogneiss from the Su-Lu terrane, eastern China. *American Mineralogist*, *80*, 475–482. <https://doi.org/10.2138/am-1995-5-608>
- Foster, G., Parrish, R. R., Horstwood, M. S. A., Chenery, S., Pyle, J. M., & Gibson, H. D. (2004). The generation of prograde P–T–t points and paths; a textural, compositional, and chronological study of metamorphic monazite, earth planet. *Science Letters*, *228*, 125–142. <https://doi.org/10.1016/j.epsl.2004.09.024>
- Gaidies, F., Morneau, Y. E., Petts, D. C., Jackson, S. E., Zagorevski, A., & Ryan, J. J. (2021). Major and trace element mapping of garnet: Unravelling the conditions, timing and rates of metamorphism of the snowcap assemblage, west-Central Yukon. *Journal of Metamorphic Geology*, *39*, 133–164. <https://doi.org/10.1111/jmg.12562>
- Ganguly, J., & Tirone, M. (1999). Diffusion closure temperature and age of a mineral with arbitrary extent of diffusion: Theoretical formulation and applications. *Earth and Planetary Science Letters*, *170*, 131–140. [https://doi.org/10.1016/S0012-821X\(99\)00089-8](https://doi.org/10.1016/S0012-821X(99)00089-8)
- Ganguly, J., Tirone, M., & Hervig, R. L. (1998). Diffusion kinetics of samarium and neodymium in garnet, and a method of determining cooling rates of rocks. *Science*, *281*, 805–807. <https://doi.org/10.1126/science.281.5378.805>
- Garber, J. M., Rioux, M., Cruz-Urbe, A. M., Smye, A. J., & Searle, M. P. (2023). Shear heating along a nascent subduction interface. Goldschmidt conference. Lyon. Abstract 20087. <https://doi.org/10.7185/gold2023.20087>
- Garber, J. M., Rioux, M., Kylander-Clark, A. R. C., Hacker, B. R., Vervoort, J. D., & Searle, M. P. (2020). Petrochronology of Wadi Tayin metamorphic sole metasediment, with implications for the thermal and tectonic evolution of the Samail ophiolite (Oman/UAE). *Tectonics*, *39*, e2020TC006135. <https://doi.org/10.1029/2020TC006135>
- García-Casco, A., Torres-Roldán, R. L., Millán, G., Monié, P., & Schneider, J. (2002). Oscillatory zoning in eclogitic garnet and amphibole, northern Serpentinite Melange, Cuba: A record of tectonic instability during subduction? *Journal of Metamorphic Geology*, *20*, 581–598. <https://doi.org/10.1046/j.1525-1314.2002.00390.x>
- George, F. R., Gaidies, F., & Boucher, B. (2018). Population-wide garnet growth zoning revealed by LA-ICP-MS mapping: Implications for trace element equilibration and syn-kinematic deformation during crystallisation. *Contributions to Mineralogy and Petrology*, *173*, 74. <https://doi.org/10.1007/s00410-018-1503-0>
- Godet, A., Guilmette, C., Labrousse, L., Davis, D. W., Smit, M. A., Cutts, J. A., Vanier, M.-A., Lafrance, I., & Charette, B. (2020). Complete metamorphic cycle and long-lived anatexis in the c. 2.1 Ga Mistinibi complex, Canada. *Journal of Metamorphic Geology*, *38*, 235–264. <https://doi.org/10.1111/jmg.12521>
- Godet, A., Guilmette, C., Labrousse, L., Smit, M. A., Cutts, J. A., Davis, D., & Vanier, M.-A. (2021). Lu–Hf garnet dating and the timing of collisions: Palaeoproterozoic accretionary tectonics revealed in the southeastern Churchill Province, trans-Hudson Orogen, Canada. *Journal of Metamorphic Geology*, *39*, 977–1007. <https://doi.org/10.1111/jmg.12599>
- Griffin, W. L., & Brueckner, H. K. (1980). Caledonian Sm–Nd ages and a crustal origin for Norwegian eclogites. *Nature*, *285*, 319–321. <https://doi.org/10.1038/285319a0>
- Guevara, V. E., MacLennan, S. A., Dragovic, B., Caddick, M. J., Schoene, B., Kylander-Clark, A. R. C., & Couëslan, C. G. (2020). Polyphase zircon growth during slow cooling from ultrahigh temperature: An example from the Archean Pikwitonei granulite domain. *Journal of Petrology*, *61*, ega021. <https://doi.org/10.1093/petrology/egaa021>
- Guilmette, C., Smit, M. A., van Hinsbergen, D. J. J., Gürer, D., Corfu, F., Charette, B., Maffione, M., Rabeau, O., & Savard, D.

- (2018). Forced subduction initiation recorded in the sole and crust of the Semail ophiolite of Oman. *Nature Geoscience*, *11*, 688–695. <https://doi.org/10.1038/s41561-018-0209-2>
- Guilmette, C., van Hinsbergen, D. J. J., Smit, M. A., Godet, A., Fournier-Roy, F., Butler, J. P., Maffione, M., Li, S., & Hodges, K. (2023). Formation of the Xigaze Metamorphic Sole under Tibetan continental lithosphere reveals generic characteristics of subduction initiation. *Communications Earth & Environment*, *4*(1), 339. <https://doi.org/10.1038/s43247-023-01007-w>
- Hacker, B. R. (1994). Rapid emplacement of young oceanic lithosphere: Argon geochronology of the Oman ophiolite. *Science*, *265*, 1563–1565. <https://doi.org/10.1126/science.265.5178.1563>
- Hacker, B. R., & Gans, P. B. (2005). Continental collisions and the creation of ultrahigh-pressure terranes: Petrology and thermochronology of nappes in the central Scandinavian Caledonides. *Geological Society of America Bulletin*, *117*, 117–134. <https://doi.org/10.1130/B25549.1>
- Hacker, B. R., Mosenfelder, J. L., & Gnos, E. (1996). Rapid emplacement of the Oman ophiolite: Thermal and geochronologic constraints. *Tectonics*, *15*, 1230–1247. <https://doi.org/10.1029/96TC01973>
- Hacker, B. R., Ratschbacher, L., Rutte, D., Stearns, M. A., Malz, N., Stübner, K., Kylander-Clark, A. R. C., Pfänder, J. A., & Everson, A. (2017). Building the Pamir-Tibet plateau—Crustal stacking, extensional collapse, and lateral extrusion in the Pamir: 3. Thermobarometry and petrochronology of deep Asian crust. *Tectonics*, *36*, 1743–1766. <https://doi.org/10.1002/2017TC004488>
- Hauri, E. H., Wagner, T. P., & Grove, T. L. (1994). Experimental and natural partitioning of Th, U, Pb and other trace elements between garnet, clinopyroxene and basaltic melts. *Chemical Geology*, *117*(1–4), 149–166. [https://doi.org/10.1016/0009-2541\(94\)90126-0](https://doi.org/10.1016/0009-2541(94)90126-0)
- Heaman, L. M., Böhm, C. O., Machado, N., Krogh, T. E., Weber, W., & Corkery, M. (2011). The Pikwitonei granulite domain, Manitoba: A giant Neoproterozoic high-grade terrane in the northwest Superior Province. *Canadian Journal of Earth Sciences*, *48*, 205–245. <https://doi.org/10.1139/E10-058>
- Hermann, J., & Rubatto, D. (2003). Relating zircon and monazite domains to garnet growth zones: Age and duration of granulite facies metamorphism in the Val Malenco lower crust. *Journal of Metamorphic Geology*, *21*, 833–852. <https://doi.org/10.1046/j.1525-1314.2003.00484.x>
- Hess, B., & Ague, J. J. (2022). Modeling diffusion-induced stresses in garnet with implications for diffusion chronometry. American Geophysical Union Fall Meeting. Abstract V52A-05
- Hickmott, D. D., Shimizu, N., Spear, F. S., & Selverstone, J. (1987). Trace-element zoning in a metamorphic garnet. *Geology*, *15*, 573–576. [https://doi.org/10.1130/0091-7613\(1987\)15<573:TZIIMG>2.0.CO;2](https://doi.org/10.1130/0091-7613(1987)15<573:TZIIMG>2.0.CO;2)
- Holder, R. M., Hacker, B. R., Kylander-Clark, A. R. C., & Cottle, J. M. (2015). Monazite trace-element and isotopic signatures of (ultra)high-pressure metamorphism: Examples from the Western gneiss region, Norway. *Chemical Geology*, *409*, 99–111. <https://doi.org/10.1016/j.chemgeo.2015.04.021>
- Holder, R. M., Yakymchuk, C., & Viete, D. R. (2020). Accessory mineral Eu anomalies in suprasolidus rocks: Beyond feldspar. *Geochemistry, Geophysics, Geosystems*, *21*, e2020GC009052. <https://doi.org/10.1029/2020GC009052>
- Hollister, L. S. (1966). Garnet zoning: An interpretation based on the Rayleigh fractionation model. *Science*, *154*, 1647–1651. <https://doi.org/10.1126/science.154.3757.1647>
- Hoover, W. F., Penniston-Dorland, S., Baumgartner, L., Bouvier, A.-S., Dragovic, B., Locatelli, M., Angiboust, S., & Agard, P. (2022). Episodic fluid flow in an eclogite-facies shear zone: Insights from Li isotope zoning in garnet. *Geology*, *50*, 746–750. <https://doi.org/10.1130/G49737.1>
- Ibañez-Mejía, M., Bloch, E., & Vervoort, J. D. (2018). Timescales of collisional metamorphism from Sm–Nd, Lu–Hf and U–Pb thermochronology: A case from the Proterozoic Putumayo Orogen of Amazonia. *Geochimica et Cosmochimica Acta*, *235*, 103–126. <https://doi.org/10.1016/j.gca.2018.05.017>
- Jamtveit, B. (1991). Oscillatory zonation patterns in hydrothermal grossular-andradite garnet: Nonlinear dynamics in regions of immiscibility. *American Mineralogist*, *76*, 1319–1327.
- Johnson, T. A., Vervoort, J. D., Ramsey, M. J., Aleinikoff, J. N., & Southworth, S. (2018). Constraints on the timing and duration of orogenic events by combined Lu–Hf and Sm–Nd geochronology: An example from the Grenville orogeny. *Earth and Planetary Science Letters*, *501*, 152–164. <https://doi.org/10.1016/j.epsl.2018.08.030>
- Kelly, E. D., Carlson, W. D., & Connelly, J. N. (2011). Implications of garnet resorption for the Lu–Hf garnet geochronometer: An example from the contact aureole of the Makhavinekh Lake pluton, Labrador. *Journal of Metamorphic Geology*, *29*, 901–916. <https://doi.org/10.1111/j.1525-1314.2011.00946.x>
- Kohn, M. J. (2004). Oscillatory- and sector-zoned garnets record cyclic (?) rapid thrusting in Central Nepal. *Geochemistry, Geophysics, Geosystems*, *5*, Q12014. <https://doi.org/10.1029/2004GC000737>
- Kohn, M. J. (2009). Models of garnet differential geochronology. *Geochimica et Cosmochimica Acta*, *73*, 170–182. <https://doi.org/10.1016/j.gca.2008.10.004>
- Kohn, M. J., Wieland, M. S., Parkinson, C. D., & Upreti, B. N. (2005). Five generations of monazite in Langtang gneisses: Implications for chronology of the Himalayan metamorphic core. *Journal of Metamorphic Geology*, *23*, 399–406. <https://doi.org/10.1111/j.1525-1314.2005.00584.x>
- Konrad-Schmolke, M., Halama, R., Chew, D., Heuzé, C., De Hoog, C. J., & Ditterova, H. (2022). Discrimination of thermodynamic and kinetic contributions to the heavy rare earth element patterns in metamorphic garnet. *Journal of Metamorphic Geology*, *41*, 465–490. <https://doi.org/10.1111/jmg.12703>
- Konrad-Schmolke, M., O'Brien, P. J., de Capitani, C., & Carswell, D. A. (2008). Garnet growth at high- and ultra-high pressure conditions and the effect of element fractionation on mineral modes and composition. *Lithos*, *103*, 309–332. <https://doi.org/10.1016/j.lithos.2007.10.007>
- Kooijman, E., Mezger, K., & Berndt, J. (2010). Constraints on the U–Pb systematics of metamorphic rutile from in situ LA-ICP-MS analysis, earth planet. *Science Letters*, *293*, 321–330. <https://doi.org/10.1016/j.epsl.2010.02.047>
- Kooijman, E., Smit, M. A., Mezger, K., & Berndt, J. (2012). Trace element systematics in granulite facies rutile: Implications for Zr geothermometry and provenance studies. *Journal of Metamorphic Geology*, *30*, 397–412. <https://doi.org/10.1111/j.1525-1314.2012.00972.x>

- Kooijman, E., Smit, M. A., Ratschbacher, L., & Kylander-Clark, A. R. C. (2017). A view into crustal evolution at mantle depths. *Earth and Planetary Science Letters*, *465*, 59–69. <https://doi.org/10.1016/j.epsl.2017.02.032>
- Kylander-Clark, A. R. C., Hacker, B. R., Johnson, C. M., Beard, B. L., Mahlen, N. J., & Lapen, T. J. (2007). Coupled Lu-Hf and Sm-Nd geochronology constrains prograde and exhumation histories of high- and ultrahigh-pressure eclogites from western Norway. *Chemical Geology*, *242*, 137–154. <https://doi.org/10.1016/j.chemgeo.2007.03.006>
- Larson, K. P., Gervais, F., & Kellett, D. A. (2013). A P-T-t-D discontinuity in east-Central Nepal: Implications for the evolution of the Himalayan mid-crust. *Lithos*, *179*, 275–292. <https://doi.org/10.1016/j.lithos.2013.08.012>
- Lasaga, A. C. (1998). *Kinetic theory in the earth sciences*. Princeton University Press. 822 p. <https://doi.org/10.1515/9781400864874>
- Lihter, I., Larson, K. P., Smit, M. A., Cottle, J. M., Ashley, K. T., & Shrestha, S. (2022). Decrypting the polymetamorphic record of the Himalaya. *Geology*, *50*, 588–592. <https://doi.org/10.1130/G49467.1>
- Martin, A. J. (2009). Sub-millimeter heterogeneity of yttrium and chromium during growth of semi-pelitic garnet. *Journal of Petrology*, *50*, 1713–1727. <https://doi.org/10.1093/ptrology/egp050>
- Mezger, K., Bohlen, S. R., & Hanson, G. N. (1990). Metamorphic history of the Archean Pikwitonei granulite domain and the cross Lake subprovince, Superior Province, Manitoba, Canada. *Journal of Petrology*, *31*, 483–517. <https://doi.org/10.1093/ptrology/31.2.483>
- Mezger, K., Essene, E. H., & Halliday, A. N. (1992). Closure temperatures of the Sm-Nd system in metamorphic garnets. *Earth and Planetary Science Letters*, *113*, 397–409. [https://doi.org/10.1016/0012-821X\(92\)90141-H](https://doi.org/10.1016/0012-821X(92)90141-H)
- Mezger, K., Hanson, G. N., & Bohlen, S. R. (1989a). U-Pb systematics of garnet: Dating the growth of garnet in the late Archean Pikwitonei granulite domain at Cauchon and Natawahunan Lakes, Manitoba, Canada. *Contributions to Mineralogy and Petrology*, *101*, 136–148. <https://doi.org/10.1007/BF00375301>
- Mezger, K., Hanson, G. N., & Bohlen, S. R. (1989b). High-precision U-Pb ages of metamorphic rutile: Application to the cooling history of high-grade terranes. *Earth and Planetary Science Letters*, *96*, 106–118. [https://doi.org/10.1016/0012-821X\(89\)90126-X](https://doi.org/10.1016/0012-821X(89)90126-X)
- Moore, S. J., Carlson, W. D., & Hesse, M. A. (2013). Origins of yttrium and rare earth element distributions in metamorphic garnet. *Journal of Metamorphic Geology*, *31*, 663–689. <https://doi.org/10.1111/jmg.12039>
- Mørk, M. B. E., & Mearns, E. W. (1986). Sm-Nd isotopic systematics of a gabbro-eclogite transition. *Lithos*, *19*, 255–267. [https://doi.org/10.1016/0024-4937\(86\)90026-5](https://doi.org/10.1016/0024-4937(86)90026-5)
- Otamendi, J. E., de la Rosa, J. D., Patiño-Douce, A. E., & Castro, A. (2002). Rayleigh fractionation of heavy rare earths and yttrium during metamorphic garnet growth. *Geology*, *30*, 159–162. [https://doi.org/10.1130/0091-7613\(2002\)030<0159:RFOHRE>2.0.CO;2](https://doi.org/10.1130/0091-7613(2002)030<0159:RFOHRE>2.0.CO;2)
- Park, C., Choi, W., Kim, H., Park, M.-H., Kang, I.-M., Lee, H.-S., & Song, Y. (2017). Oscillatory zoning in skarn garnet: Implications for tungsten ore exploration. *Ore Geology Reviews*, *89*, 1006–1018. <https://doi.org/10.1016/j.oregeorev.2017.08.003>
- Paton, C., Hellstrom, J., Paul, B., Woodhead, J., & Hergt, J. (2011). Iolite: Freeware for the visualisation and processing of mass spectrometric data. *Journal of Analytical Atomic Spectrometry*, *26*, 2508–2518. <https://doi.org/10.1039/C1JA10172B>
- Pattison, D. R. M., De Capitani, C., & Gaidies, F. (2011). Petrological consequences of variations in metamorphic reaction affinity. *Journal of Metamorphic Geology*, *29*, 953–977. <https://doi.org/10.1111/j.1525-1314.2011.00950.x>
- Paul, B., Paton, C., Norris, A., Woodhead, J., Hellstrom, J., Hergt, J., & Greig, A. (2012). CellSpace: A module for creating spatially registered laser ablation images within the Iolite free-ware environment. *Journal of Analytical Atomic Spectrometry*, *27*, 700–706. <https://doi.org/10.1039/C2JA10383D>
- Percival, J. A., Sanborn-Barrie, M., Skulski, T., Stott, G. M., Helmstaedt, H., & White, D. J. (2006). Tectonic evolution of the western Superior Province from NATMAP and Lithoprobe studies. *Canadian Journal of Earth Sciences*, *43*, 1085–1117. <https://doi.org/10.1139/e06-062>
- Pourteau, A., Smit, M. A., Li, Z.-X., Collins, W. J., Nordsvan, A. R., Volante, S., & Li, J. (2018). 1.6 Ga crustal thickening along the final Nuna suture. *Geology*, *46*, 959–962. <https://doi.org/10.1130/G45198.1>
- Pownall, J. M., Armstrong, R. A., Williams, I. S., Thirlwall, M. F., Manning, C. J., & Hall, R. (2019). *Miocene UHT granulites from Seram, eastern Indonesia: A geochronological-REE study of zircon, monazite and garnet*. Special Publication (Vol. 478) (pp. 167–196). Geological Society of London. <https://doi.org/10.1144/SP478.8>
- Pyle, J. M., & Spear, F. (2000). An empirical garnet (YAG) - Xenotime thermometer. *Contributions to Mineralogy and Petrology*, *138*, 51–58. <https://doi.org/10.1007/PL00007662>
- Raimondo, T., Payne, J., Wade, B., Lanari, P., Clark, C., & Hand, M. (2017). Trace element mapping by LA-ICP-MS: Assessing geochemical mobility in garnet. *Contributions to Mineralogy and Petrology*, *172*, 17. <https://doi.org/10.1007/s00410-017-1339-z>
- Räss, L., Utkin, I., Duretz, T., Omlin, S., & Podladchikov, Y. Y. (2022). Assessing the robustness and scalability of the accelerated pseudo-transient method. *Geoscientific Model Development*, *15*, 5757–5786. <https://doi.org/10.5194/gmd-15-5757-2022>
- Regis, D., Warren, C. J., Mottram, C. M., & Roberts, N. M. W. (2016). Using monazite and zircon petrochronology to constrain the P-T-t evolution of the middle crust in the Bhutan Himalaya. *Journal of Metamorphic Geology*, *34*, 617–639. <https://doi.org/10.1111/jmg.12196>
- Rioux, M., Bowring, S., Kelemen, P., Gordon, S., Miller, R., & Dudás, F. (2013). Tectonic development of the Samail ophiolite: High-precision U-Pb zircon geochronology and Sm-Nd isotopic constraints on crustal growth and emplacement. *Journal of Geophysical Research - Solid Earth*, *118*, 2085–2101. <https://doi.org/10.1002/jgrb.50139>
- Root, D. B., Hacker, B. R., Gans, P. B., Ducea, M. N., Eide, E. A., & Mosenfelder, J. L. (2005). Discrete ultrahigh-pressure domains in the Western gneiss region, Norway: Implications for formation and exhumation. *Journal of Metamorphic Geology*, *23*, 45–61. <https://doi.org/10.1111/j.1525-1314.2005.00561.x>
- Rubatto, D. (2002). Zircon trace element geochemistry: Partitioning with garnet and the link between U-Pb ages and metamorphism. *Chemical Geology*, *184*, 123–138. [https://doi.org/10.1016/S0009-2541\(01\)00355-2](https://doi.org/10.1016/S0009-2541(01)00355-2)



- Rubatto, D., Burger, M., Lanari, P., Hattendorf, B., Schwarz, G., Neff, C., Schmidt, P. T., Hermann, J., Vho, A., & Günther, D. (2020). Identification of growth mechanisms in metamorphic garnet by high-resolution trace element mapping with LA-ICP-TOFMS. *Contributions to Mineralogy and Petrology*, 175, 61. <https://doi.org/10.1007/s00410-020-01700-5>
- Rubatto, D., & Hermann, J. (2007). Experimental zircon/melt and zircon/garnet trace element partitioning and implications for the geochronology of crustal rocks. *Chemical Geology*, 241, 38–61. <https://doi.org/10.1016/j.chemgeo.2007.01.027>
- Scherer, E. E., Cameron, K. L., & Blichert-Toft, J. (2000). Lu–Hf garnet geochronology: Closure temperature relative to the Sm–Nd system and the effects of trace mineral inclusions. *Geochimica et Cosmochimica Acta*, 64, 3413–3432. [https://doi.org/10.1016/S0016-7037\(00\)00440-3](https://doi.org/10.1016/S0016-7037(00)00440-3)
- Schmidt, J., Hacker, B. R., Ratschbacher, L., Stübner, K., Stearns, M. A., Kylander-Clark, A. R. C., Cottle, J. M., Webb, A. A. G., Gehrels, G. E., & Minaev, V. N. (2011). Cenozoic deep crust in the Pamir. *Earth and Planetary Science Letters*, 312, 411–421. <https://doi.org/10.1016/j.epsl.2011.10.034>
- Schumacher, R., Roetzler, K., & Maresch, W. V. (1999). Subtle oscillatory zoning in garnet from regional metamorphic phyllites and mica schists, western Erzgebirge, Germany. *The Canadian Mineralogist*, 37, 381–403.
- Scoates, J. S., Scoates, R. F. J., Wall, C. J., Friedman, R. M., & Couëslan, C. G. (2017). Direct dating of ultramafic sills and mafic intrusions associated with Ni-sulfide mineralization in the Thompson Nickel Belt, Manitoba, Canada. *Economic Geology*, 112, 675–692. <https://doi.org/10.2113/econgeo.112.3.675>
- Searle, M., & Cox, J. (1999). Tectonic setting, origin, and obduction of the Oman ophiolite. *Geological Society of America Bulletin*, 111, 104–122. [https://doi.org/10.1130/0016-7606\(1999\)111<0104:TSAOO>2.3.CO;2](https://doi.org/10.1130/0016-7606(1999)111<0104:TSAOO>2.3.CO;2)
- Searle, M., & Malpas, J. (1980). Structure and metamorphism of rocks beneath the Semail ophiolite of Oman and their significance in ophiolite obduction. *Trans. Royal Soc. Edinburgh: Earth Sci.*, 71, 247–262. <https://doi.org/10.1017/S0263593300013614>
- Shannon, R. D. (1976). Revised effective ionic radii and systematic studies of interatomic distances in halides and chalcogenides. *Acta Crystallographica. Section a*, 32, 751–767. <https://doi.org/10.1107/S0567739476001551>
- Simpson, A., Gilbert, S., Tamblyn, R., Hand, M., Spandler, C., Gillespie, J., Nixon, A., & Glorie, S. (2021). In-situ Lu–Hf geochronology of garnet, apatite and xenotime by LA-ICP-MS/MS. *Chemical Geology*, 577, 120299. <https://doi.org/10.1016/j.chemgeo.2021.120299>
- Skora, S., Baumgartner, L. P., Mahlen, N. J., Johnson, C. M., Pilet, S., & Hellebrand, E. (2006). Diffusion-limited REE uptake by eclogite garnets and its consequences for Lu–Hf and Sm–Nd geochronology. *Contributions to Mineralogy and Petrology*, 152, 703–720. <https://doi.org/10.1007/s00410-006-0128-x>
- Smit, M. A., Hacker, B. R., & Lee, J. (2014). Tibetan garnet records early Eocene initiation of thickening in the Himalaya. *Geology*, 42, 591–594. <https://doi.org/10.1130/G35524.1>
- Smit, M. A., Ratschbacher, L., Kooijman, E., & Stearns, M. A. (2014). Early evolution of the Pamir deep crust from Lu–Hf and U–Pb geochronology and garnet thermometry. *Geology*, 42, 1047–1050. <https://doi.org/10.1130/G35878.1>
- Smit, M. A., Scherer, E. E., John, T., & Janssen, A. (2011). Creep of garnet in eclogite: Mechanisms and implications. *Earth and Planetary Science Letters*, 311, 411–419. <https://doi.org/10.1016/j.epsl.2011.09.024>
- Smit, M. A., Scherer, E. E., & Mezger, K. (2013a). Lu–Hf and Sm–Nd garnet geochronology: Chronometric closure and implications for dating petrological processes. *Earth and Planetary Science Letters*, 381, 222–233. <https://doi.org/10.1016/j.epsl.2013.08.046>
- Smit, M. A., Scherer, E. E., & Mezger, K. (2013b). Peak metamorphic temperatures from cation diffusion zoning in garnet. *Journal of Metamorphic Geology*, 31, 339–358. <https://doi.org/10.1111/jmg.12024>
- Soret, M., Agard, P., Dubacq, B., Plunder, A., & Yamato, P. (2017). Petrological evidence for stepwise accretion of metamorphic soles during subduction infancy (Semail ophiolite, Oman and UAE). *Journal of Metamorphic Geology*, 35, 1051–1080. <https://doi.org/10.1111/jmg.12267>
- Soret, M., Bonnet, G., Agard, P., Larson, K. P., Cottle, J. M., Dubacq, B., Kylander-Clark, A. R. C., Button, M., & Rividi, N. (2022). Timescales of subduction initiation and evolution of subduction thermal regimes. *Earth and Planetary Science Letters*, 584, 117521. <https://doi.org/10.1016/j.epsl.2022.117521>
- Spear, F. S. (2017). Garnet growth after overstepping. *Chemical Geology*, 466, 491–499. <https://doi.org/10.1016/j.chemgeo.2017.06.038>
- Stearns, M. A., Hacker, B. R., Ratschbacher, L., Lee, J., Cottle, J. M., & Kylander-Clark, A. R. C. (2013). Synchronous Oligocene–Miocene metamorphism of the Pamir and the north Himalaya driven by plate-scale dynamics. *Geology*, 41, 1071–1074. <https://doi.org/10.1130/G34451.1>
- Stearns, M. A., Hacker, B. R., Ratschbacher, L., Rutte, D., & Kylander-Clark, A. R. C. (2015). Titanite petrochronology of the Pamir gneiss domes: Implications for middle to deep crust exhumation and titanite closure to Pb and Zr diffusion. *Tectonics*, 34, 784–802. <https://doi.org/10.1002/2014TC003774>
- Stowell, H., Zuluaga, C., Boyle, A., & Bulman, G. (2011). Garnet sector and oscillatory zoning linked with changes in crystal morphology during rapid growth, north cascades, Washington. *American Mineralogist*, 96, 1354–1362. <https://doi.org/10.2138/am.2011.3759>
- Stübner, K., Ratschbacher, L., Rutte, D., Stanke, K., Minaev, V., Wiesinger, M., Gloaguen, R., & Project TIPAGE members. (2013). The giant Shakh-dara migmatitic gneiss dome, Pamir, India-Asia collision zone: 1 geometry and kinematics. *Tectonics*, 32, 948–979. <https://doi.org/10.1002/tect.20057>
- Stübner, K., Ratschbacher, L., Weise, C., Chow, J., Hofmann, J., Khan, J., Rutte, D., Sperner, B., Pfänder, J., Hacker, B. R., Dunkl, I., Tichimirowa, M., Stearns, M. A., & Project TIPAGE members. (2013). The giant Shakh-dara migmatitic gneiss dome, Pamir, India-Asia collision zone: 2 timing of dome formation. *Tectonics*, 32, 1404–1431. <https://doi.org/10.1002/tect.20059>
- Tamblyn, R., Hand, M., Simpson, A., Gilbert, S., Wade, B., & Glorie, S. (2021). In situ laser ablation Lu–Hf geochronology of garnet across the Western gneiss region: Campaign-style dating of metamorphism. *Journal of the Geological Society of London*, 179, jgs2021–094. <https://doi.org/10.1144/jgs2021-094>

- Taylor, R. J. M., Harley, S. L., Hinton, R. W., Elphick, S., Clark, C., & Kelly, N. M. (2015). Experimental determination of REE partition coefficients between zircon, garnet and melt: A key to understanding high-T crustal processes. *Journal of Metamorphic Geology*, 33, 231–248. <https://doi.org/10.1111/jmg.12118>
- Terry, M. P., Robinson, P., Hamilton, A., & Jercinovic, M. J. (2000). Monazite geochronology of UHP and HP metamorphism, deformation, and exhumation, Nordøyane, Western gneiss region, Norway. *American Mineralogist*, 85, 1651–1664. <https://doi.org/10.2138/am-2000-11-1208>
- Terry, M. P., Robinson, P., & Krogh-Ravna, E. J. (2000). Kyanite eclogite thermobarometry and evidence for thrusting of UHP over HP metamorphic rocks, Nordøyane, Western gneiss region, Norway. *American Mineralogist*, 85, 1637–1650. <https://doi.org/10.2138/am-2000-11-1207>
- Thiessen, E. J., Gibson, H. D., Regis, D., Pehrsson, S. J., Cutts, J. A., & Smit, M. A. (2019). High-grade metamorphism flying under the radar of accessory minerals. *Geology*, 47, 568–572. <https://doi.org/10.1130/G45979.1>
- Tirone, M., Ganguly, J., Dohmen, R., Langenhorst, F., Hervig, R., & Becker, H.-W. (2005). Rare earth diffusion kinetics in garnet: Experimental studies and applications. *Geochimica et Cosmochimica Acta*, 69, 2385–2398. <https://doi.org/10.1016/j.gca.2004.09.025>
- Tsujimori, T., Sisson, V. B., Liou, J. G., Harlow, G. E., & Sorensen, S. S. (2006). Petrologic characterization of Guatemalan lawsonite eclogite: Eclogitization of subducted oceanic crust in a cold subduction zone. In B. R. Hacker & W. C. McClelland (Eds.), *Ultrahigh-pressure metamorphism: Deep continental subduction* (Vol. 403) (pp. 147–168). Geol. Soc. Am. Spec. Paper. [https://doi.org/10.1130/2006.2403\(09](https://doi.org/10.1130/2006.2403(09)
- Tual, L., Smit, M. A., Kooijman, E., Kielman-Schmitt, M., & Ratschbacher, L. (2022). Garnet, zircon, and monazite age and REE signatures in (ultra)high-temperature and high-pressure rocks: Examples from the Caledonides and the Pamir. *Journal of Metamorphic Geology*, 40, 1321–1346. <https://doi.org/10.1111/jmg.12667>
- van Orman, J. A., Grove, T. L., Shimizu, N., & Layne, G. D. (2002). Rare earth element diffusion in a natural pyrope single crystal at 2.8 GPa. *Contributions to Mineralogy and Petrology*, 142, 416–424. <https://doi.org/10.1007/s004100100304>
- Viete, D. R., Hacker, B. R., Allen, M. B., Seward, G. G. E., Tobin, M. J., Kelley, C. S., Cinque, G., & Duckworth, A. R. (2018). Metamorphic records of multiple seismic cycles during subduction. *Science Advances*, 4, eaaq0234. <https://doi.org/10.1126/sciadv.aaq0234>
- Wain, A. (1997). New evidence for coesite in eclogite and gneisses: Defining an ultrahigh-pressure province in the Western gneiss region of Norway. *Geology*, 25, 927–930. [https://doi.org/10.1130/0091-7613\(1997\)025<0927:NEFCIE>2.3.CO;2](https://doi.org/10.1130/0091-7613(1997)025<0927:NEFCIE>2.3.CO;2)
- Walczak, K., Anczkiewicz, R., Szczepański, J., Rubatto, D., & Košler, J. (2017). Combined garnet and zircon geochronology of the ultra-high temperature metamorphism: Constraints on the rise of the Orlica-Snieżnik dome, NE Bohemian Massif, SW Poland. *Lithos*, 292–293, 388–400. <https://doi.org/10.1016/j.lithos.2017.09.013>
- Walczak, K., Cuthbert, S., Kooijman, E., Majka, J., & Smit, M. A. (2019). U–Pb zircon age dating of diamond-bearing gneiss from Fjortoft reveals repeated burial of the Baltoscandian margin during the Caledonian orogeny. *Geological Magazine*, 156, 1949–1964. <https://doi.org/10.1017/S0016756819000268>
- Warren, C. J., Greenwood, L. V., Argles, T. W., Roberts, N. M. W., Parrish, R. R., & Harris, N. B. W. (2019). Garnet–monazite rare earth element relationships in sub-solidus metapelites: A case study from Bhutan. *Special Publication. Geological Society of London*, 478, SP4781. <https://doi.org/10.1144/SP478.1>
- Weber, W., & Scoates, R. F. J. (1978). Archean and Proterozoic metamorphism in the northwestern Superior Province and along the Churchill-Superior boundary, Manitoba. In J. A. Fraser & W. W. Heywood (Eds.), *Metamorphism in the Canadian shield* (Vol. 78–10) (pp. 5–16). Geol. Survey Can. Paper. <https://doi.org/10.4095/104516>
- Wilbur, D. E., & Ague, J. J. (2006). Chemical disequilibrium during garnet growth: Monte Carlo simulations of natural crystal morphologies. *Geology*, 34(8), 689. <https://doi.org/10.1130/g22483.1>

**How to cite this article:** Smit, M. A., Vrijmoed, J. C., Scherer, E. E., Mezger, K., Kooijman, E., Schmitt-Kielman, M., Tual, L., Guilmette, C., & Ratschbacher, L. (2024). Retentiveness of rare earth elements in garnet with implications for garnet Lu-Hf chronology. *Journal of Metamorphic Geology*, 1–25. <https://doi.org/10.1111/jmg.12769>